NIST GCR 96-690

Preliminary Processing of the Lotung LSST Data

Building and Fire Research Laboratory
Gaithersburg, MD 20899

United States Department of Commerce
Technology Administration
National Institute of Standards and Technology

NIST GCR 96-690

Preliminary Processing of the Lotung LSST Data

Steven D. Glaser
Alena L. Leeds

Division of Engineering
Colorado School of Mines
Golden, CO 80401

March 1996
Building and Fire Research Laboratory
National Institute of Standards and Technology
Gaithersburg, MD 20899

U.S. Department of Commerce
Ronald H. Brown, *Secretary*
Technology Administration
Mary L. Good, *Under Secretary for Technology*
National Institute of Standards and Technology
Arati Prabhakar, *Director*

Abstract

Possibly the best set of data for earthquake excitation of soils exists for the test site operated by the Electric Power Research Institute (EPRI) and the Taiwan Power Company at Lotung Taiwan. At this site, two locations are instrumented with three-component accelerometers at depths of 47, 17, 11, 6 meters, and at the surface. One array is in the free-field while the other is adjacent to a one-quarter scale nuclear containment vessel. The site is also well instrumented with piezometers at various depths and locations. The simplified soil profile consists of 30 to 35 m of silty sand and sandy silt with some gravel, overlaying a thick clay and silt deposit. The water table is within half a meter of the ground surface. This area is seismically active, and strong shaking generated by many earthquakes exhibiting a wide range of magnitudes have been recorded since 1986.

This report summarizes the data and signal processing that was done to the EPRI Lotung data at the Colorado School of Mines. The over 2000 files were organized into MATLAB experiments by event. The provided acceleration data were carefully double integrated to yield velocity and displacement time history records. The data are now in proper format to begin system identification analysis.

Acknowledgments

We would like to thank the Electric Power Research Institute, in particular H. T. Tang, for making the data available through a Cooperative R&D Agreement with the National Institute of Standards and Technology (NIST). We also want to thank Riley Chung and Ron Andrus at the Structures Division, NIST for providing technical support. This study was funded by NIST under Contract No. 60NANB4D1677.

Contents

CHAPTER 1 - INTRODUCTION

1.1 Background

There are many unanswered questions of interest to the geotechnical community concerning the behavior of soils subjected to earthquake excitation. Foremost among them are questions concerning the strain-dependent non-linear behavior of soils, and soil-structure interaction. In an attempt to gain further rational understanding of these problems the Electric Power Research Institute (EPRI), and Colorado School of Mines (CSM), and the Structures Division of the National Institute of Standards and Technology (NIST) formed a cooperative research team to evaluate ground motion time histories recorded at the Lotung site, Taiwan.

Much of the necessary data is to be made available by EPRI from the Lotung site. The Lotung strong motion data set are an extremely unique set of data. The completeness of this input-output data set makes it ideal for analysis using system identification (SI) methods. Data from the Wildlife Site, Imperial Valley CA, and Treasure Island are freely available. This report lays out the work undertaken by the P.I. at CSM for 1994, with funding provided by NIST under Award Number 60NANB4D1677.

1.2 Why Use System Identification?

An important goal for earthquake engineering is the ability to estimate soil properties without intruding into the soil mass. For the engineer interested in seismic behavior of soils, the dynamic properties of the soil are of interest, particularly large-strain properties. The archetypal large strain field excitation is earthquake strong motion. Ideally, both ground motions into the soil layer of interest and on the surface above the layer are recorded, as illustrated by the cartoon in Fig. 1.1. Given this known input propagating upward from depth, and the output at the top of the soil column, the behavior of the soil can be modelled by inverse theory. If a suitable model is chosen to represent the system of interest, the estimated model parameters will correspond to important mechanical parameters of the system, such as damping, natural frequency, and stiffness. This estimation of parameters is commonly known as system identification (SI).

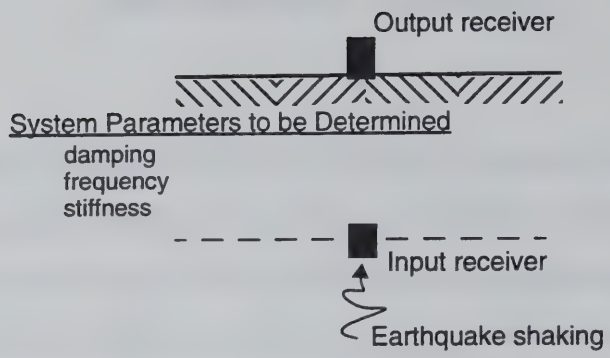

Fig. 1.1 - Configuration of the System Identification Method.

The traditional method of geotechnical analysis of dynamic soil motions is through the Fourier transform. However, serious problems arise when this method is applied to short data streams, and to signals changing through time — non-stationary signals. This study was undertaken to show the effectiveness of a different type of model, a parametric model commonly used in automatic control and geophysics, which avoids many of the limitations inherent with calculating the system transfer function by Fourier techniques. An important aspect of particular parametric models is the theoretical link between the estimated system parameters and the mechanical parameters of a lumped-mass oscillator. The parametric model allows estimates of system dynamic properties to be to be made if an input-output data set is available.

1.3 Scope

The purpose of this report is to set the stage for future detailed SI analyses of the Lotung site. To this end the Lotung site itself will be introduced through geological, seismological, and geotechnical description. The method of data processing used to prepare the ground acceleration and pore water pressure time records will be discussed in detail. Finally a brief example of SI analysis on an individual record will be presented to illustrate the method to be used.

CHAPTER 2 - THE LOTUNG SITE, TAIWAN

2.1 Introduction and Geography

With the growth of the use of nuclear-powered generating plants in the 1970's, many safety related questions about the seismic performance of these plants arose. In the early 1980's, EPRI and the Taiwan Power Co. (TPC) constructed two scale models (1/4 and 1/12 scale) of a nuclear containment structure near Lotung, Taiwan. This is a very seismically active area in northeast Taiwan (see Fig. 2.1). The site and structures were elaborately instrumented so that soil and structural response, and soil-structure interaction, to earthquakes could be carefully studied (Tang et al., 1989; Liu and Yeh, 1985).

2.2 Instrumentation

The soil instrumentation includes a three-arm surface array, as shown in Fig. 2.2. The arms radiate approximately 47 m from the 1/4 scale containment structure. In addition, there are two downhole arrays of accelerometers extending to a depth of 47 m, as shown in Fig. 2.2. The surface accelerometers are triaxial force-balance units (Kinemetrics FBA-13) oriented in the N-S, E-W, and vertical directions. The downhole arrays (DHA and DHB) are modified Kinemetrics FBA-13H units oriented in the N-S, E-W, and vertical directions. DHA is located 3 m from the containment vessel and DHB is located 47 m from the structure, allowing identification of the effects of the structure on soil response. The downhole instruments are located at depths of 6, 11, 17, and 47 m. The simplified soil profile consists of 30-35 m of silty sand and sandy silt with some gravel, above clayey silt and silty clay. The water table is within half a meter of the ground surface.

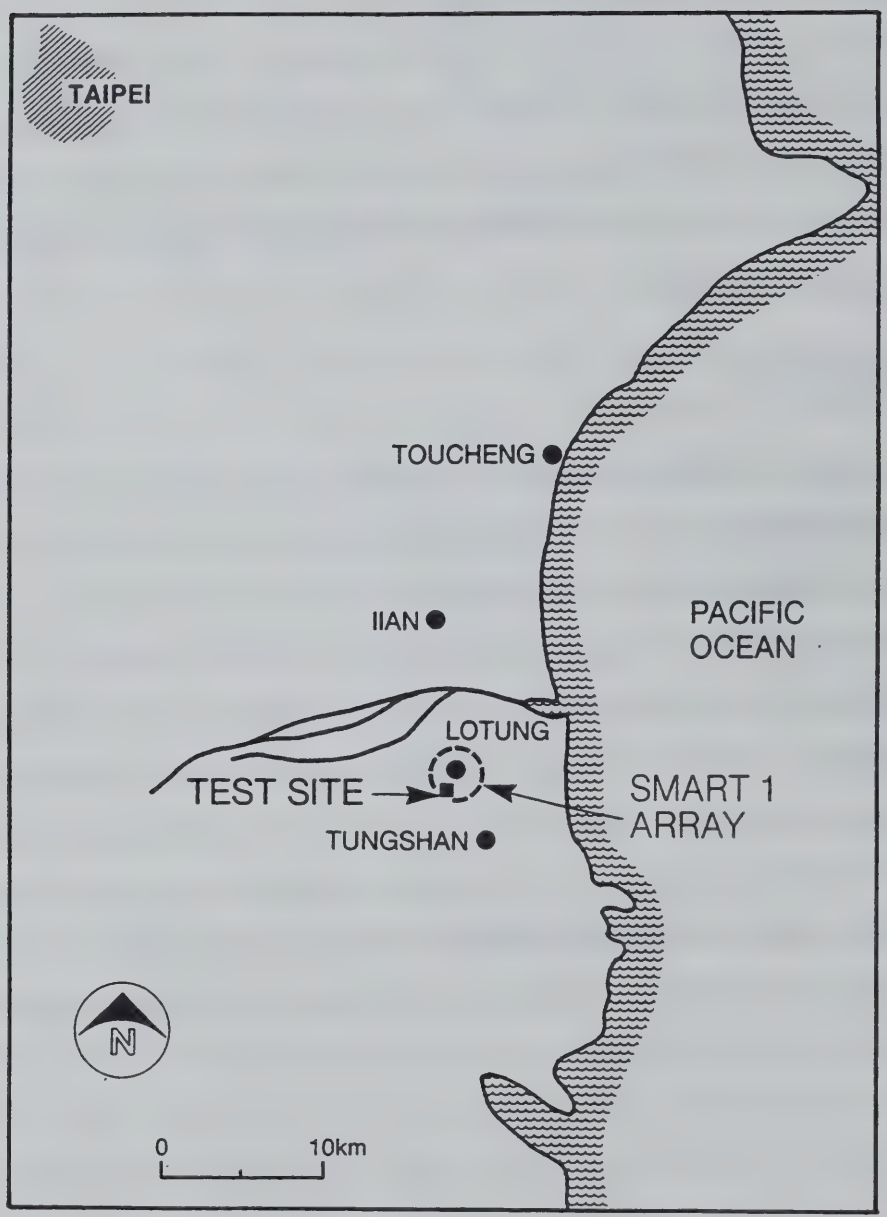

Fig. 2.1 Location of Lotung Large-Scale Seismic Test Site (LSST). EPRI (1989)

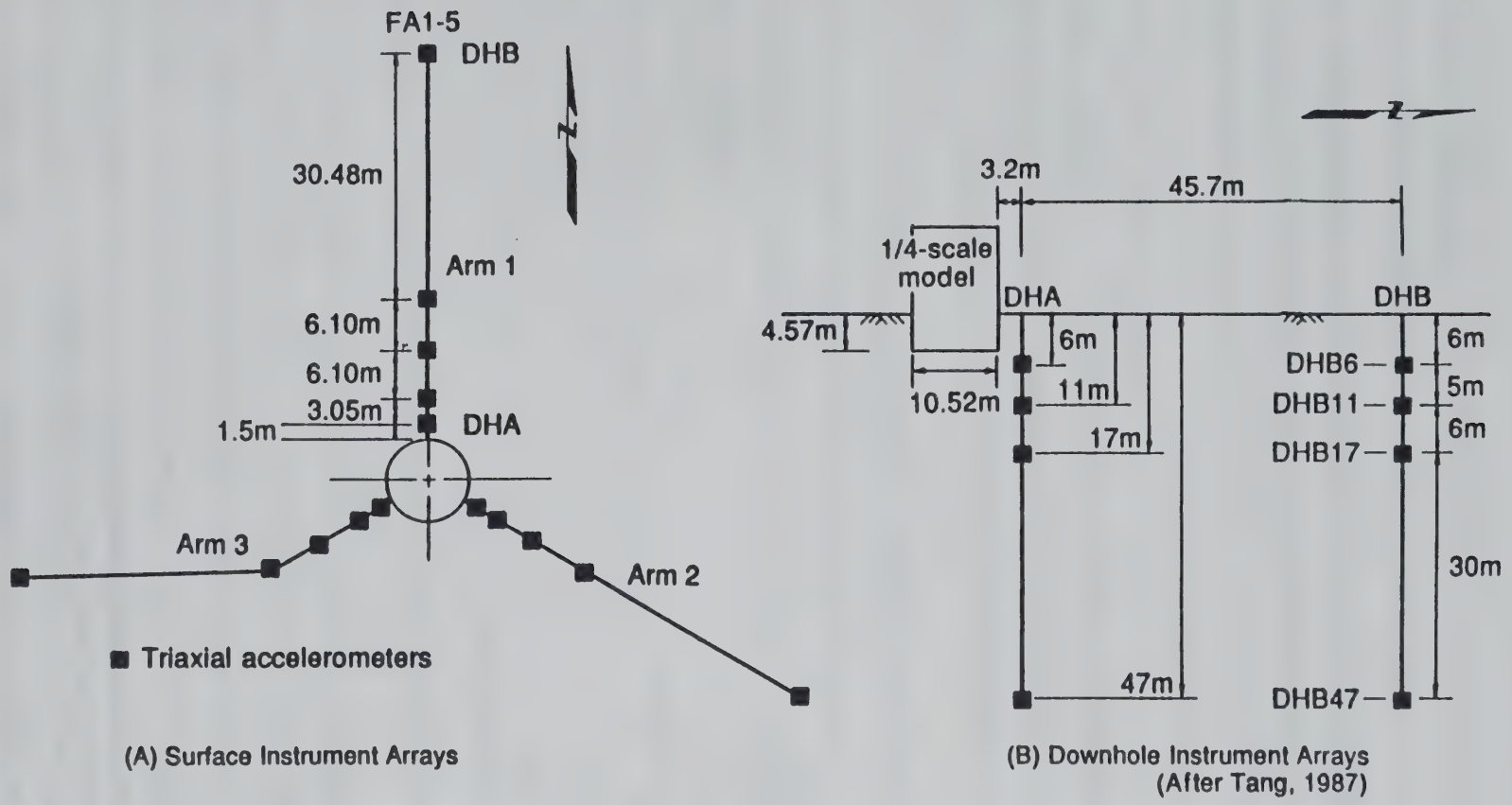

Fig. 2.2 Location of surface and downhole instrumentation Chang, et al (1991)

2.3 Site Characterization

The basic geology of the LSST site is summarized by Wen and Yeh (1984) and Tang (1987). The area consists of a recent alluvium layer 40 to 50 m thick overlying a Pleistocene formation that varies from 150 to 500 m in thickness. Underlying the Pleistocene material is a Miocene basement rock. Characteristic geological profiles also showing compressional wave velocities are shown in Fig. 2.3. Example soil profiles are shown on Fig. 2.4. The locations of the boreholes from which the profiles were constructed are shown on Fig. 2.5.

Five stages of laboratory testing programs were performed at the LSST during specific phases of the project to determine engineering properties of the soil. A summary of the tests performed is included here and the specific references for the test results are given below.

1. 1984 Jong Shing Boring Services (JSBS) Laboratory Testing Program

   Index properties:
   - Soil classification
   - Grain size analyses
   - Moisture contents
   - Specific gravity
   - Dry density and void ratio
   - Atterberg limits

   Engineering properties:
   - Direct shear tests
   - Triaxial shear tests
   - Unconfined compression tests

2. 1987 National Taiwan University (NTU) Laboratory Testing Program

   Index properties:
   - Grain size analyses
   - Moisture content
   - Specific gravity
   - Dry density
   - Atterberg limits

   Engineering properties:
   - Uniaxial - load/unload and cyclic loading tests
   - Triaxial - compression, extension and cyclic loading tests
   - Resonant column
   - Hydrostatic - load/unload and cyclic loading tests
   - Compaction tests

3. 1987 University of California at Davis (UCD) Laboratory Testing Program

Engineering properties:
- Triaxial shear loading
- Cyclic triaxial liquefaction testing

This phase of the laboratory testing was performed in conjunction with the installation of pore water pressure transducers at the site. Pore water pressures were monitored in the samples during these laboratory tests.

4. 1989 NTU Laboratory Testing Program

Engineering properties:
- One dimensional rebound
- Resonant column
- Cyclic triaxial liquefaction
- Permeability
- Cyclic triaxial modulus

These additional tests were performed by NTU for the specific purpose of investigating the form of the shear modulus versus shearing strain and material damping versus shearing strain curves for undisturbed soil samples.

5. 1990 UCD Laboratory Testing Program

Engineering properties:
- Cyclic triaxial modulus
- Cyclic triaxial liquefaction
- Cyclic simple shear
- One dimensional rebound
- Permeability

These tests by UCD were independent of the 1989 NTU tests and were performed to investigate discrepancies in modulus and damping data found from analysis of 1987 results for the LSST site. In addition, it provided additional data on the cyclic strength and liquefaction properties of the soil. Blowcount results from the SPT are shown on Fig. 2.6 for 2 of the 3 drilling and sampling programs. The appearance of an occasional layer requiring an excess of 50 blows per foot indicates a gravelly soil zone that occurs in discrete lenses rather than as a consistent layer. Results of CPT soundings are shown in Fig. 2.7 and 2.8. Occasional spikes in tip resistance values confirm the presence of the gravelly lenses.

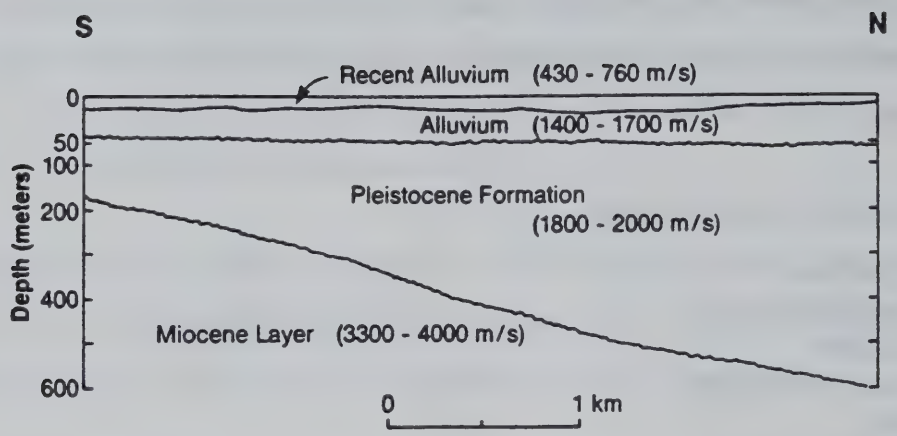

a) Geological Profile and Compressional Wave Velocity Along North-South Section

After Tang (1)

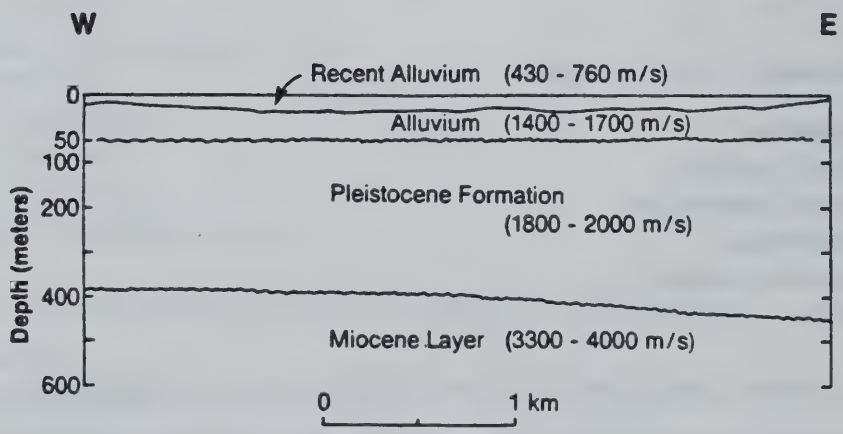

b) Geological Profile and Compressional Wave Velocity Along East-West Section

Fig. 2.3 Geological profiles for the Lotung site. EPRI (1989)

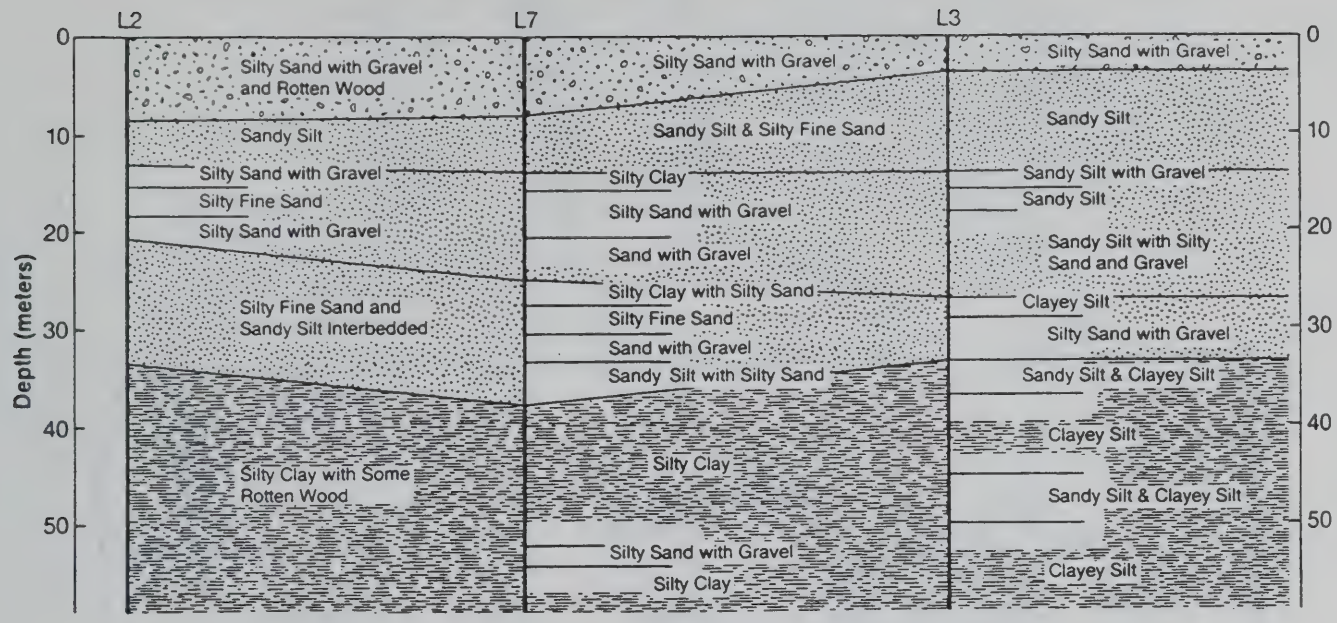

PROFILE I

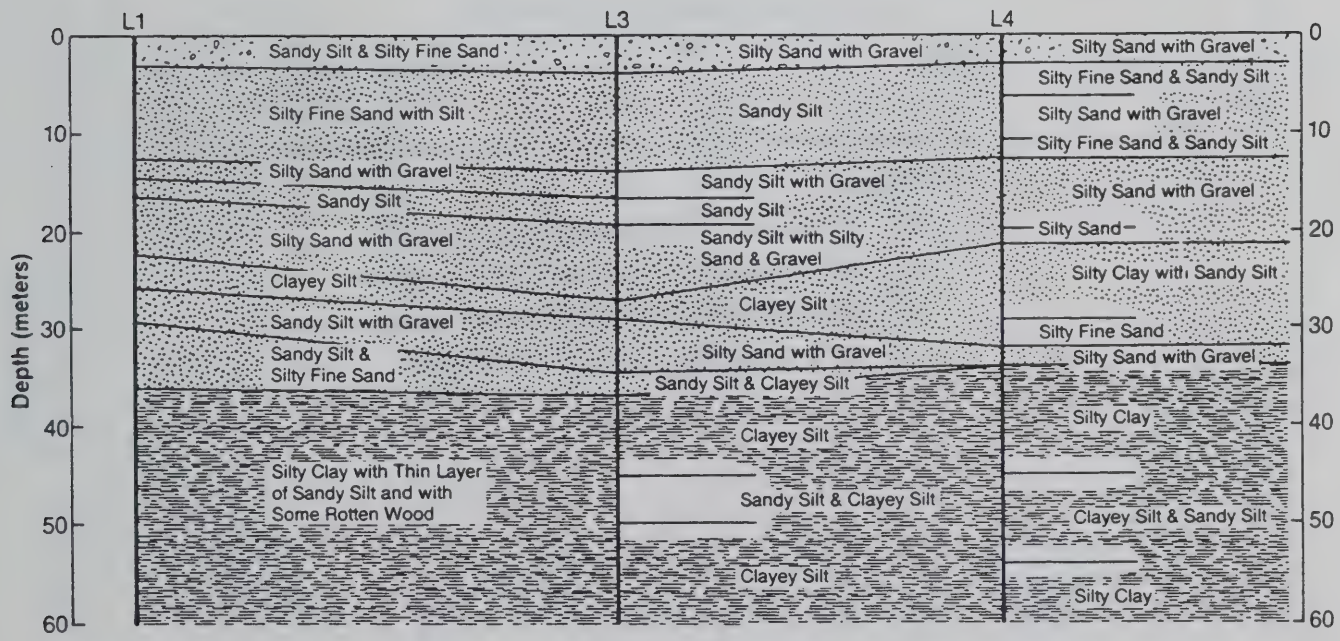

PROFILE II

After NTU (4)

Fig. 2.4 Detailed soil profiles developed during the WECC field program. EPRI (1989)

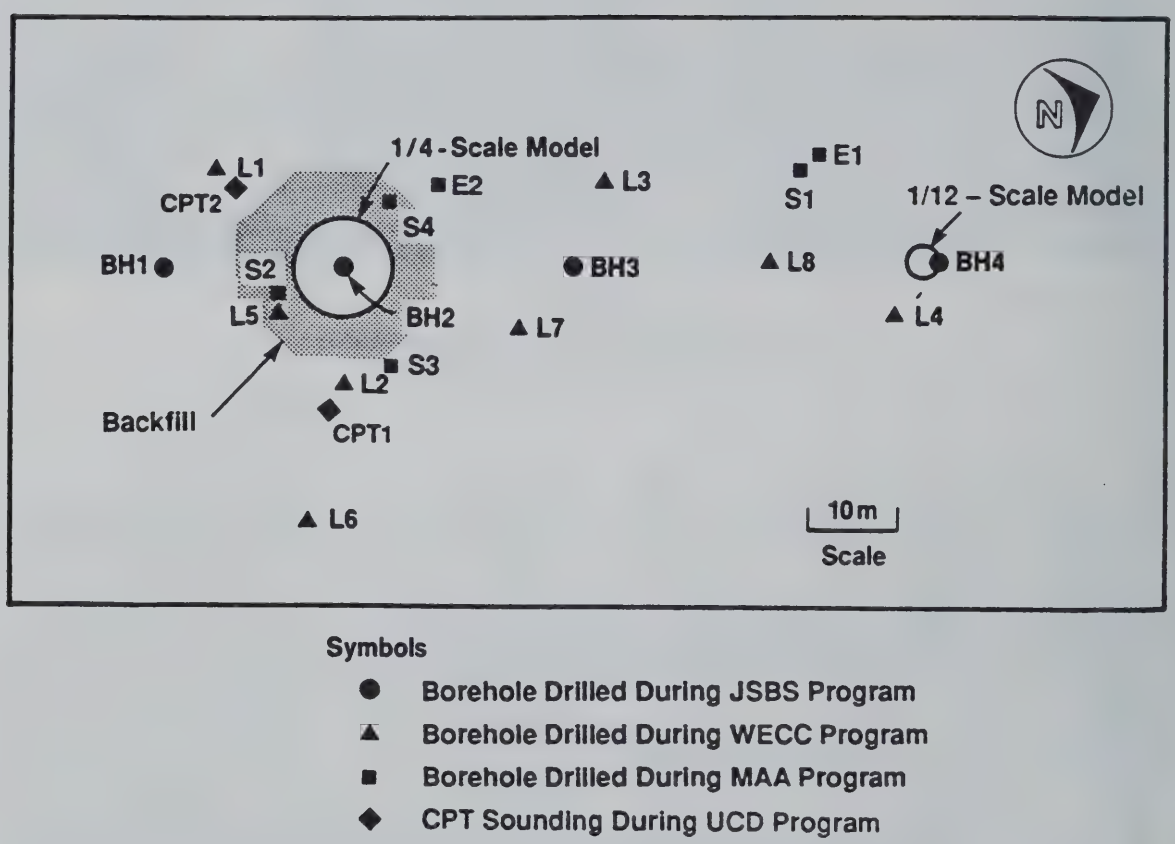

Fig. 2.5 Location of boreholes at the Lotung site, and location of soil profiles. Anderson (1993)

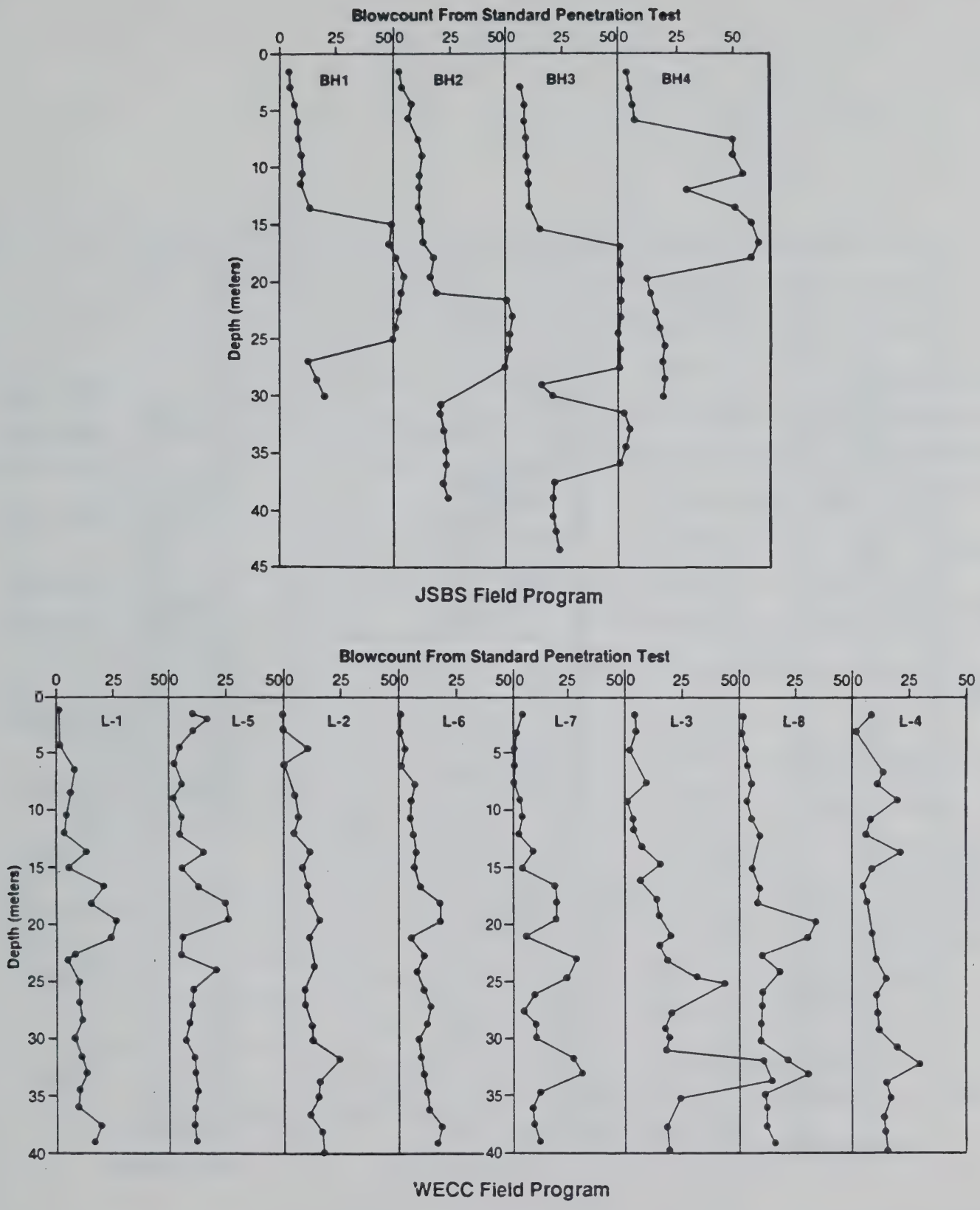

Fig. 2.6 SPT blowcounts recorded at Lotung test site. Anderson (1993)

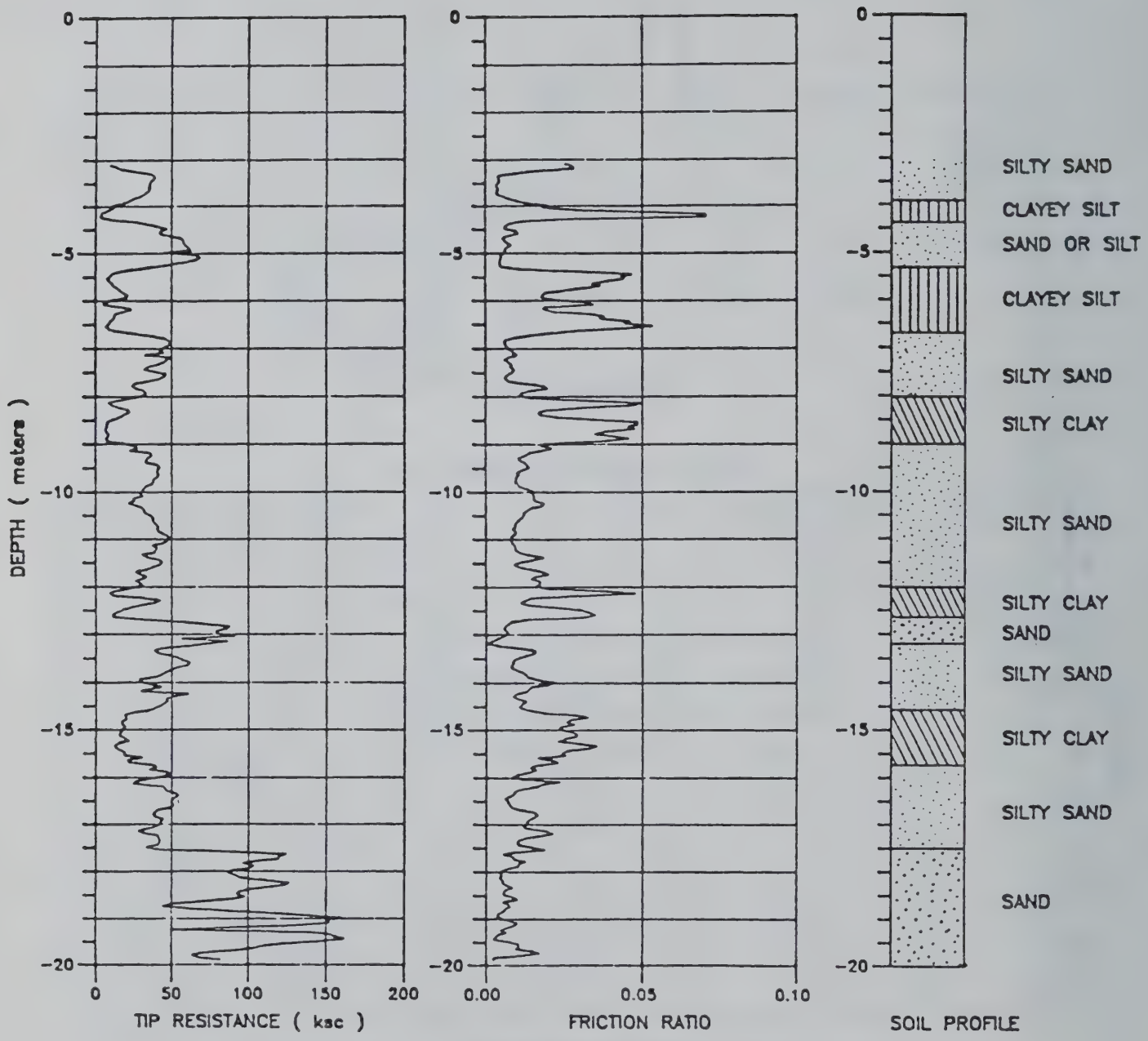

Fig. 2.7 CPT tip resistance, friction ratio and estimated soil profile at test hole #1. Anderson (1993)

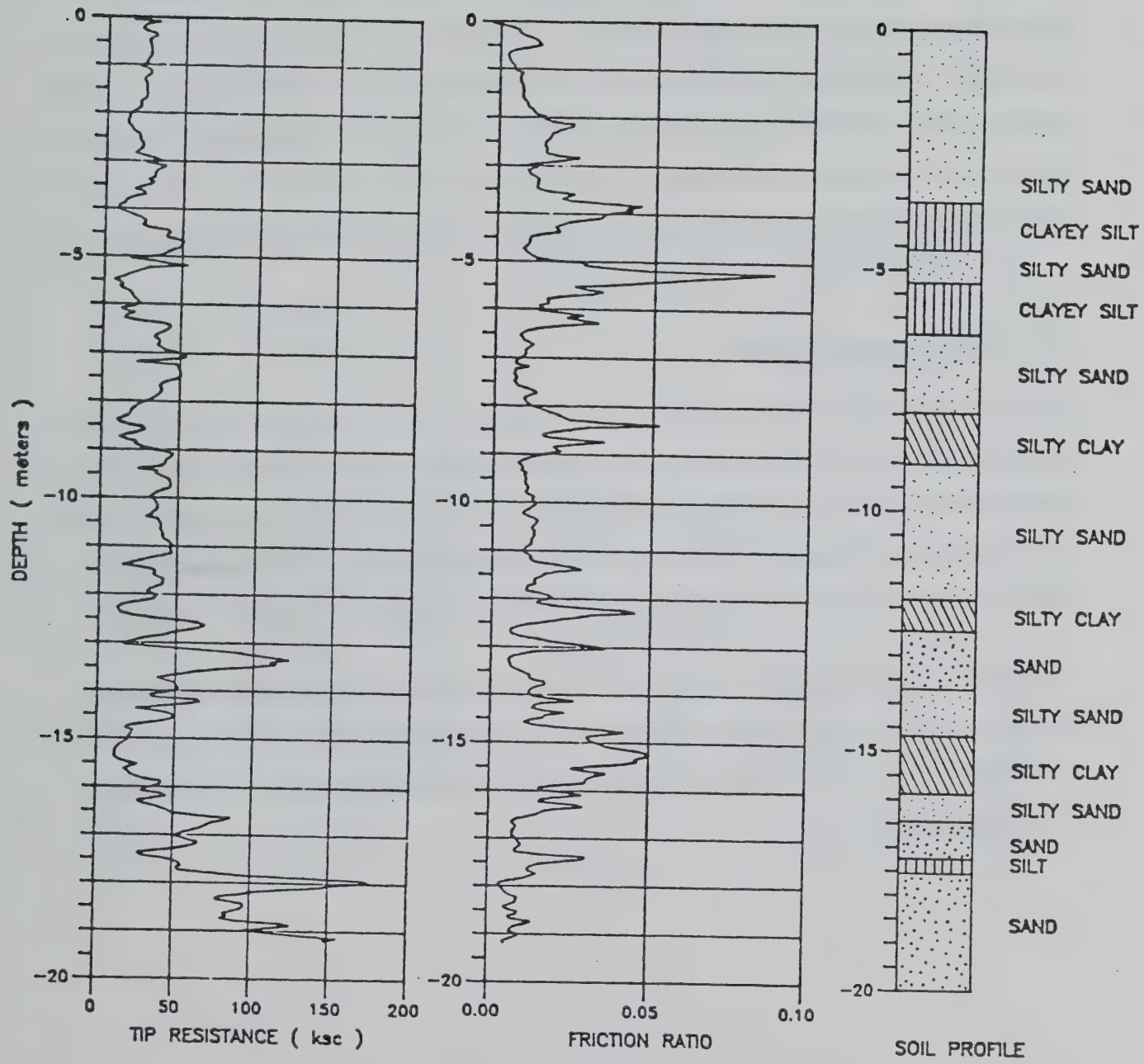

Fig. 2.8 CPT tip resistance, friction ratio and estimated soil profile at test hole #2. Anderson (1993)

2.4 Seismology

A summary of the properties of measured temblors is given in Table 2.1. The epicenters for these events is shown on the map presented in Fig. 2.9. For the initial interpretation work it was decided to concentrate on the events for which accurate pore pressure records exist and show some increase in pore pressure during strong shaking. Events 12, 16, and 17 meet this criteria. Events 12 and 16 were major events and have been discussed in detail (e.g. EPRI, 1989; Chang et al., 1991; Anderson, 1993). Event 17 is an aftershock of event 16 which generated enough pore pressure to register on the recording equipment. The time histories for acceleration, velocity, and displacement for Event 16 are shown in Fig. 3.1, with a full velocity records given in Appendix A.

2.5 Pore Pressure Generation

Over the history of the Lotung experiment, 0ver 30 pore water pressure transducers were installed at the site (Shen et al., 1989). The location of these sensors in relation to the three-arm surface array is shown in Fig. 2.10. The soil conditions at several pertinent locations are given in Table 2.2. As reported by Shen et al. (1989), most of the sensors ailed due to mechanical problems. However, several remained in operating condition and were triggered by events 12, 16, and 17.

A typical pore pressure record is shown in Fig. 2.11 in relation to the acceleration time history. Information as to in situ pore pressure and increase for each sensor for events 12, 16, and 17 are given in Tables 2.3, 2.4, and 2.5, respectively. The time histories from events 12, 16, and 17 are given in Appendix B.

Event No.	Date	Magnitude	Epicentral Distance	Focal Depth	Peak Acceleration		
					E-W	N-S	V
LSST 1	9/20/85				—	—	—
LSST 2	10/26/85	5.3 M_l			0.03 g	0.03 g	0.01 g
LSST 3	11/ 7/85	5.5 M_l			0.01 g	0.01 g	0.01 g
LSST 4	1/16/86	6.5 M_l			0.47 g	0.49 g	0.10 g
LSST 5	3/29/86				0.04 g	0.03 g	0.03 g
LSST 6	4/ 8/86	5.4 M_l	31.4 km	10.9 km	0.04 g	0.03 g	0.01 g
LSST 7	5/20/86	6.5 M_l	66.2 km	15.8 km	0.16 g	0.21 g	0.04 g
LSST 8	5/20/86	6.2 M_l	69.2 km	21.8 km	0.03 g	0.03 g	0.01 g
LSST 9	7/11/86	4.5 M_l	5.0 km	1.1 km	0.07 g	0.05 g	0.01 g
LSST 10	7/16/86	4.5 M_l	6.1 km	0.9 km	0.03 g	0.04 g	0.02 g
LSST 11	7/17/86	5.0 M_l	6.0 km	2.0 km	0.07 g	0.10 g	0.04 g
LSST 12	7/30/86	6.2 M_l	5.2 km	1.6 km	0.16 g	0.19 g	0.20 g
LSST 13	7/30/86	6.2 M_l			0.05 g	0.03 g	0.02 g
LSST 14	8/ 5/86	4.9 M_l			0.05 g	0.03 g	0.02 g
LSST 15	11/14/86				0.02 g	0.04 g	0.05 g
LSST 16	11/14/86	7.0 M_l	77.9 km	6.9 km	0.13 g	0.17 g	0.10 g
LSST 17	11/14/86				0.04 g	0.04 g	0.02 g
LSST 18	11/15/86				0.03 g	0.02 g	0.01 g

Table 2.1 Properties of the recorded LSST series of earthquakes.
After EPRI (1989) and Anderson (1993)

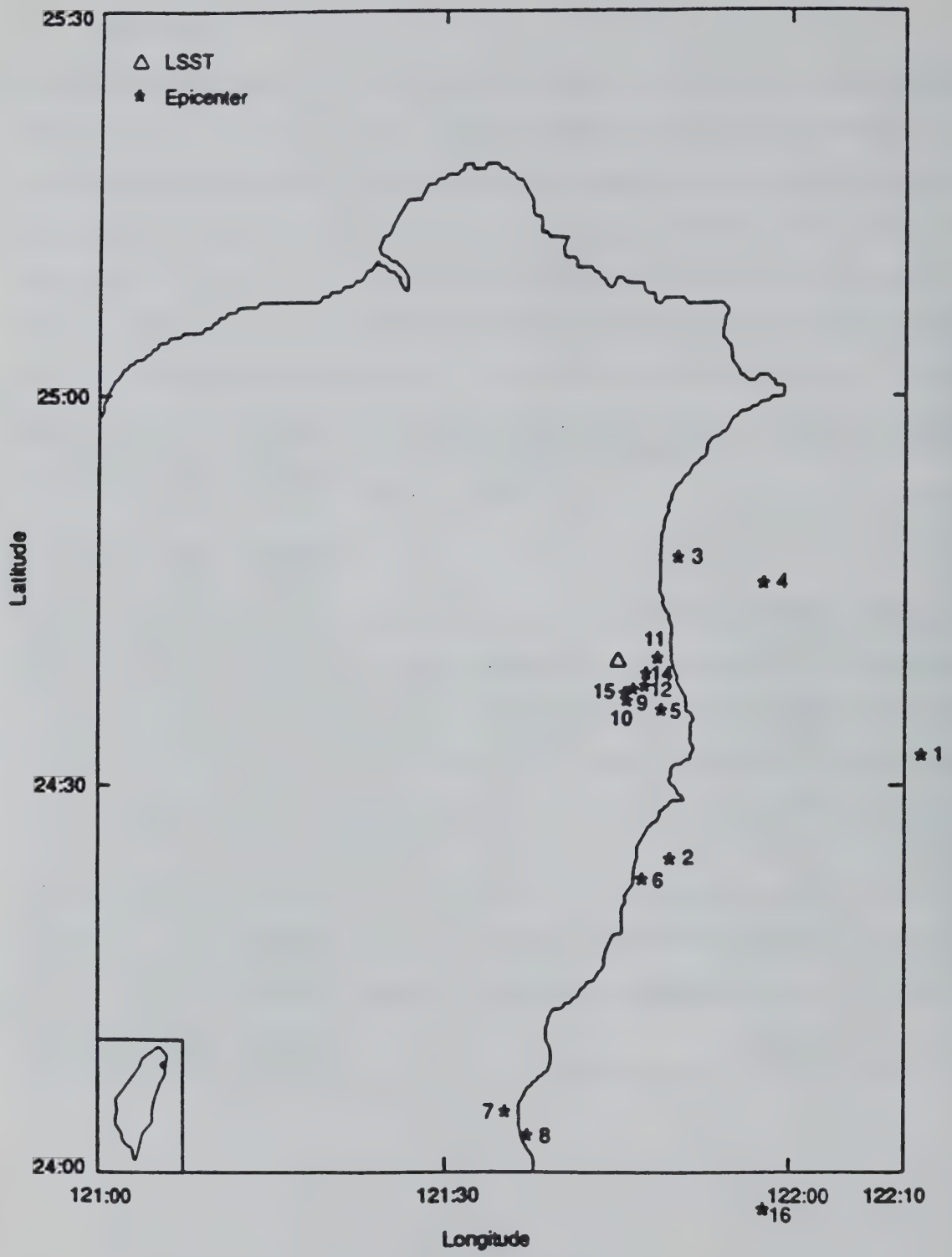

Note: The epicentral locations for Events LSST Nos. 13, 17 and 18 were not determined.

Fig. 2.9 Locations of the epicenters for LSST seismic events 1 through 18. Tang, et al (1992)

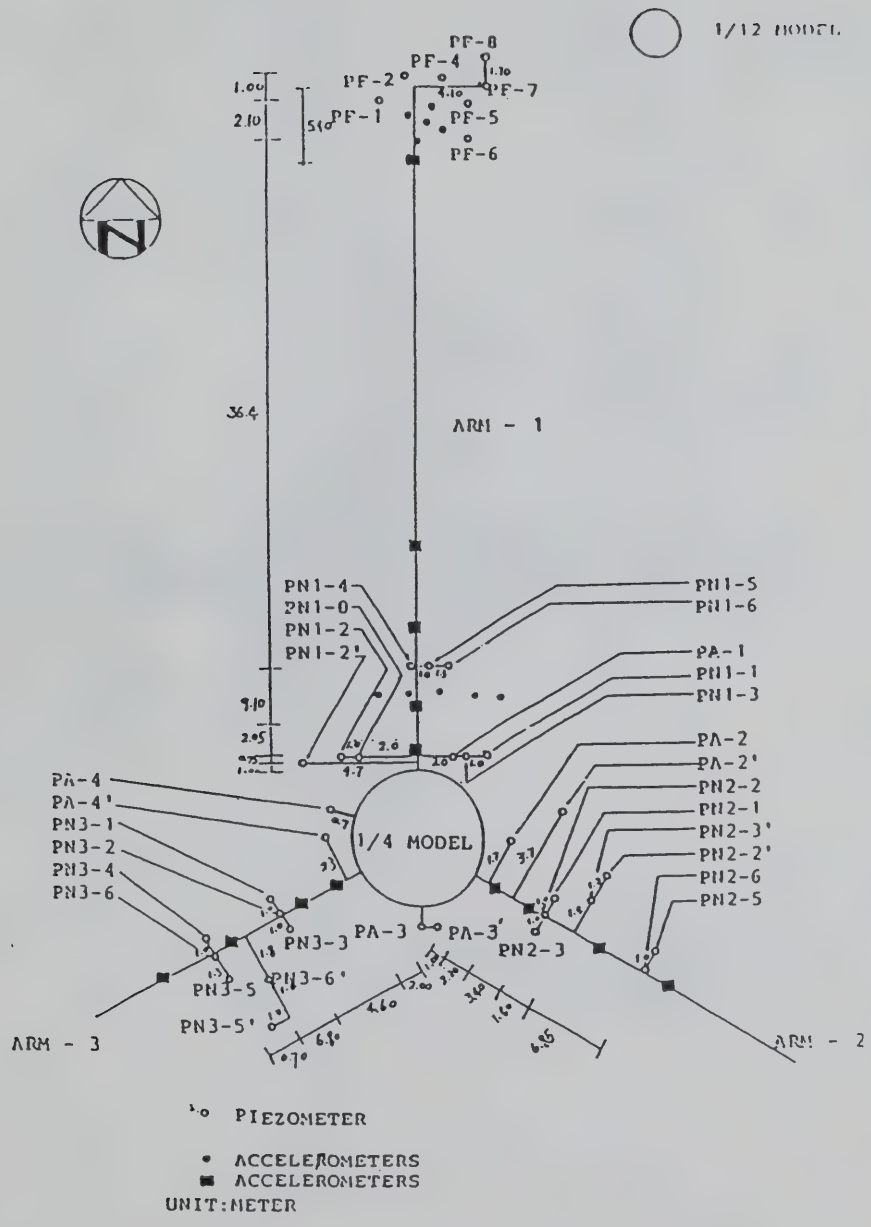

Fig. 2.10 Location of the pore water pressure sensors ant the Lotung test site. EPRI (1989)

PA-1	W(%)
F = 15.2 SM+G	7.8
CH 1 D = 5.06M T = ML F =68.5% R = 9	37.8
F = 14.6 SM	

PN1-0	W(%)
F = 10.9 SM+G	12.4
CH 11 D = 3.16M T = ML F = 92.4% R = 5.5	40
F = 50.2 ML-CL	27.0

PN2-1	W(%)
F = 10.1 SM	15.9
CH 18 D = 6.30M T = SM F = 19.5% R = 16.5 (23)	14.6
F = 42.7 SM	28.3

PN3-2	W(%)
F = 97.3 CL	34.3
CH 29 D = 11.0M T = ML F = 68.6% R = 3	31.2
F = 31.7 SM	35.8

PF-1	W(%)
F = 10.9 SM-SC	12.4
CH 5 D = 3.25M T = ML F = 56.3% R = 18	40
F = 50.2 ML	27.0

PN1-1	W(%)
F = 15.2 CL	7.8
CH 12 D = 6.03M T = SM F = 43.8% R = 25.5	37.8
F = 14.6 SM	24.3

PA-3'	W(%)
F = 8.6 SM+G	7.2
CH 21 D = 5.10M T = SM+G F = 32.0% R = 17 (20.4)	21.5

W: water content
F: fine-grained fraction
R: $\Delta u/u_0$ (%)
D: depth of sensor
T: soil type

PF-5	W(%)
F = 92.7 SM	33.3
CH 9 D = 12.0M T = ML F = 65.5% R = 3	31.6
F = 26.9 SM	21.9

PF-2	W(%)
F = 92.4 CL-ML	40
CH 6 D = 6.05M T = ML F = 50.2% R = 4	68
F = 57.0 CL-ML	32.3

PN3-1	W(%)
F = 47.6 SM-SC	21.4
CH 24 D = 6.30M T = SM F = 39.9% R = 12 (12.4)	32.7
F = 64.9 ML	31.2

PN2-2'	W(%)
F = 10.1 SM	15.9
CH 23 D = 8.00M T = SM F = 19.5% R = 4.3	14.6
F = 42.7 SM	28.3

Table 2.2 Soil conditions at the locations of pore water sensors. EPRI (1989)

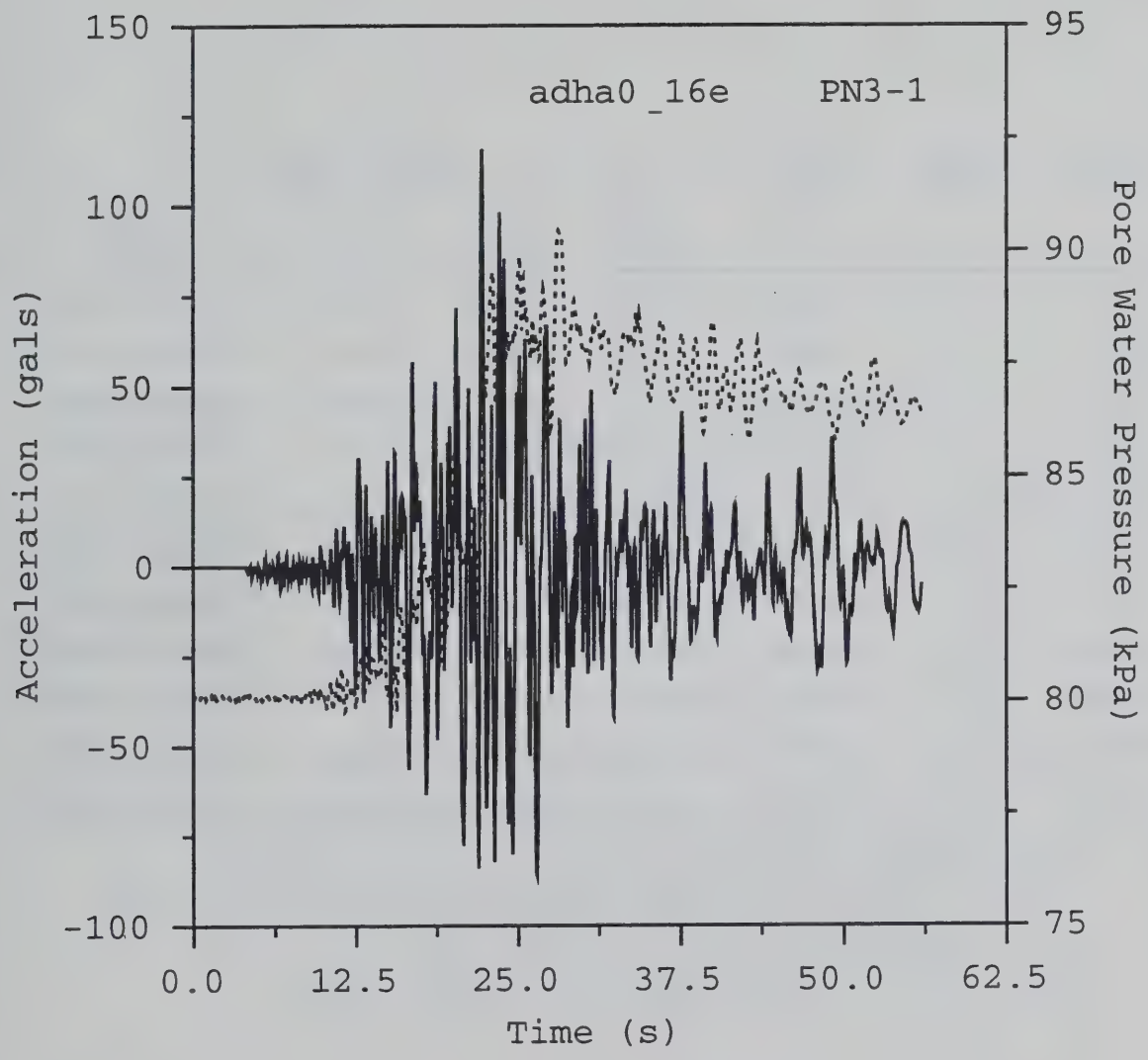

Fig. 2.11 Typical pore pressure record from event 16, LSST. Depth = 6.38 m; initial hydrostatic pressure = 72.6 kPa; increase in pore water pressure = 8.68 kPa.

Sensor No.	Channel No.	Depth, h (m)	Event LSST12			
			u_o[2] (kPa)	u_p[3] (kPa)	Δu[4] (kPa)	File Name
PA-1	1	5.06	54.60	59.90	5.30	E12C01.PWP
PF-1	5	3.25	32.80	38.97	6.17	E12C05.PWP
PF-2	6	6.05	55.70	57.67	1.97	E12C06.PWP
PF-5	9	12.00	121.85	126.14	4.29	E12C09.PWP
PN1-0	11	3.16	39.72	42.12	2.40	E12C11.PWP
PN1-1	12	6.03	61.30	78.35	17.05	E12C12.PWP
PN1-4	15	5.53	62.34	65.53	3.19	E12C15.PWP
PN2-1	18	6.30	62.12	73.36	11.24	E12C18.PWP
PA-3'	21	5.10	56.15	69.88	13.73	E12C21.PWP
PN3-1	24	6.38	72.60	81.28	8.68	E12C24.PWP
PN3-2	29	11.00	116.60	123.41	6.81	E12C29.PWP

Notes: (1) This table was modified from reference (2).
(2) u_o = Hydrostatic pressure based on initial readings of the recordings.
(3) u_p = Recorded peak pore water pressure.
(4) $\Delta u = u_p - u_o$ = Peak induced pore water pressure.

Table 2.3 Peak pore water pressures, event 12. Tang, et al (1992)

Sensor No.	Channel No.	Depth, h (m)	Event LSST16			
			u_o[2] (kPa)	u_p[3] (kPa)	Δu[4] (kPa)	File Name
PF-8	17	15.00	114.60	135.35	20.75	E16C17.PWP
PN2-1	18	6.30	66.90	83.60	16.70	E16C18.PWP
PA-3'	21	5.10	56.30	68.74	12.44	E16C21.PWP
PN2-2'	23	8.00	97.20	106.61	9.41	E16C23.PWP
PN3-1	24	6.38	80.10	90.44	10.34	E16C24.PWP

Notes: (1) This table was modified from reference (2).
(2) u_o = Hydrostatic pressure base on initial readings of the recordings.
(3) u_p = Recorded peak pore water pressure.
(4) $\Delta u = u_p - u_o$ = Peak induced pore water pressure.

Table 2.4 Peak pore water pressures, event 16. Tang, et al (1992)

Sensor No.	Channel No.	Depth, h (m)	Event LSST17			
			u_o(2) (kPa)	u_p(3) (kPa)	Δu(4) (kPa)	File Name
PF-8	17	15.00	114.60	128.73	14.13	E17C17.PWP
PN2-1	18	6.30	66.90	72.77	5.87	E17C18.PWP
PA-3'	21	5.10	56.30	61.08	4.78	E17C21.PWP
PN2-2'	23	8.00	97.20	101.92	4.72	E17C23.PWP
PN3-1	24	6.38	80.10	84.48	4.38	E17C24.PWP

Notes: (1) This table was modified from reference (2).
(2) u_o = Hydrostatic pressure based on initial readings of event LSST16 recordings.
(3) u_p = Recorded peak pore water pressure.
(4) $\Delta u = u_p - u_o$ = Peak induced pore water pressure.

Table 2.5 Peak pore water pressures, event 17. Tang, et al (1992)

Chapter 3 - Procedures for Data Processing and System Identification

3.1 Data Processing

3.1.1 Cataloging

The EPRI-supplied data consists of 10 pc-format floppy disks of data. The data supplies ground motions, structural motions, dynamic earth pressure, and ancillary data for 18 earthquake events (Tang and Tang, 1992). The data set consists of 2,103 individual files. Pore water pressure values are available for events 12, 16, and 17 only. As an example of the state of the "raw" supplied data, the complete set of "raw" ground motions and pore pressure time histories for event 16 is presented in Appendices A and B, respectively.

The first step of the data processing was to enter the relevant data files into MATLAB and group them into corresponding event files. Files event01 through event18 were created. A simplified naming convention was developed for each data record. The first letter of the name is an a, v, or d, for acceleration, velocity, and displacement, respectively. The next three letters are dha or dhb for downhole array a or b. The following number refers to the depth in meters - 0, 6, 11, 17, and 47. The second number, following the underscore refers to the event number. The last letter - e, n, or u, refers to accelerometer orientation - east-west, north-south, or up-down.

An example of the naming convention is adha47_18u. This record is the acceleration time history at a depth of 47 m at downhole array a, event 18. The record gives the vertical ground motion for this location and event.

3.1.2 Filtering, Resampling, and Integration

The data as received from EPRI is in the form of raw acceleration records, which we processed following standard U.S.G.S. method (Converse and Brady, 1992). The acceleration records are digitized at a rate of 200 samples per second (ss), for a bandwidth of 100 Hz. This relatively high Nyquist frequency causes the event records to be very long, 8,000 data points for each 40 s trace. In addition, there is little useful information for our study above 10-15 Hz, and this region would be very noisy. Resampling greatly reduces the amount of data to be later analyzed, and eliminates time-domain aliasing of the band-passed signals. It was therefore decided to low-pass filter and

resample the data at a rate of 25 ss, yielding a Nyquist frequency of 12.5 Hz. Previous work indicated that the information of interest would be contained in this band (Glaser, 1993, 1995a,b).

The data was resampled using the *resample* algorithm from the MATLAB Signal Processing Toolbox (Krauss et al., 1994). The data is first low-pass filtered using a Kaiser-windowed linear-phase FIR filter using ten terms on either side of the timestep in the calculation. The low-pass filter is applied both forward and reverse to eliminate phase shift, and the data resampled at 25 Hz. The same process was carried out for every strong motion record as well as for the pore water pressure records.

The acceleration records were then processed and integrated to provide velocity records, and the velocity records similarly reprocessed and integrated to yield displacement time histories. The procedure used to accomplish these transformations is presented in Appendix C. The acceleration record is first high-pass filtered at 0.15 Hz using a 4th order bi-directional Butterworth filter to remove dc offset and low frequency drift. A best-fit straight line from the arrival of the strong motion is then subtracted from the data, followed by the sample mean. The pre-arrival data is then set to zero. The processed acceleration data is now integrated using the trapezoidal method (Converse and Brady, 1992). The same steps are carried out on this newly formed velocity time history to yield the strong motion displacement. A typical set of processed ground motion records is shown in Fig. 3.1.

3.2 System Identification

3.2.1 Parametric Modelling

The goal of system identification is to model a system in a manner that provides needed mechanical information about that system. The most common techniques have evolved from electrical and mechanical engineering, and involve solving the inverse problem for the system transfer function. Each method has limitations; in the words of G. E. P. Box, "All models are incorrect, but some are more useful than others."

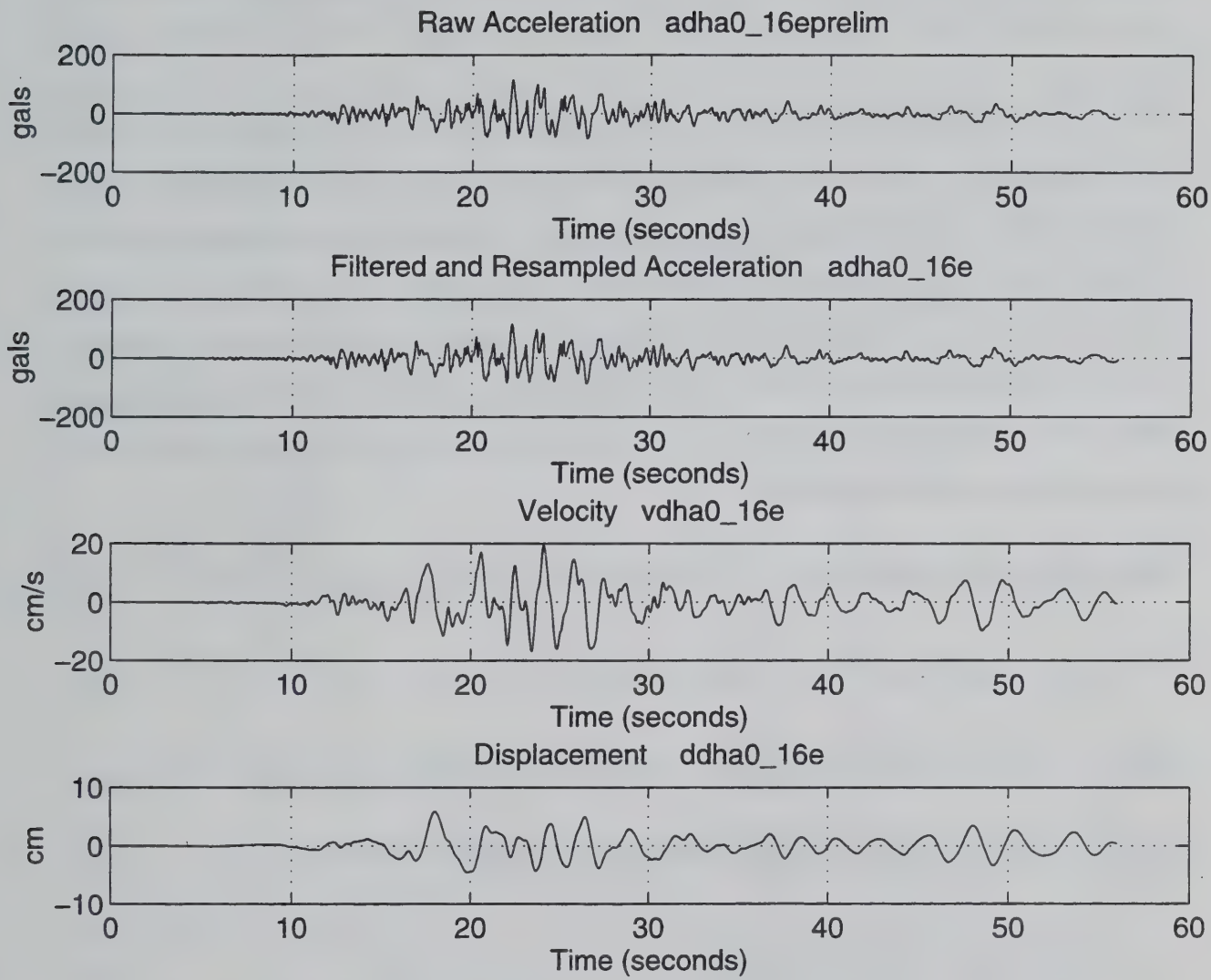

Fig. 3.1 Typical ground motion record set at Lotung, east-west component of the surface of downhole array a, event 16.

The process of inversion allows the estimation of the system response function (filter) if the input and output signals are known. A simple model for characterizing a system is as a parametric relationship between system input and output. Such a model, referred to as an autoregressive-moving average (ARMA) model, is based on discrete time series analysis:

$$y_t = a_1 y_{t-1} + a_2 y_{t-2} + \ldots + b_0 x_t + b_1 x_{t-1} + \ldots \equiv \left(\sum_{j=0}^{nb} b_j x_{t-j} + \sum_{k=1}^{na} a_k y_{t-k} \right) \qquad (1)$$

where y_j is the actual output data sequence, x_j is the input sequence (assume white noise for simple spectral estimation), *na* and *nb* are the AR and MA orders, respectively, and the subscript is the time step counter. The output is seen as a combination of the input history acted upon by the "*b*" coefficients plus the past outputs acted upon by the "*a*" coefficients. The input series, involving the "*b*" coefficients, is a causal moving average (MA) process (convolutional). The series involving weighted past output values ("*a*" coefficients) is a noncausal autoregressive (AR) process. The lengths of the AR and MA processes (model order) must be explicitly chosen so that the model best represents the process.

Applying the shifting theorem to Eq. 1. yields the Fourier transform (Bracewell, 1978)

$$Y_\omega \left(1 + a_1 e^{i\omega} + a_2 e^{2i\omega} + \ldots \right) = X_\omega \left(b_0 + b_1 e^{i\omega} + b_2 e^{2i\omega} + \ldots \right) \qquad (2)$$

where i is $\sqrt{-1}$ and ω is circular frequency. Applying the Z-transform (Bracewell, 1978), where $z^k = e^{ki\omega}$, and rearranging, yields the frequency domain transfer function H_ω

$$H_\omega = \frac{Y_\omega}{X_\omega} = \frac{b_o + b_1 z^1 + b_2 z^2 + \ldots}{1 - a_1 z^1 - a_2 z^2 + \ldots} \qquad (3)$$

The ARMA model is very powerful in that it can easily model sharp drops, sharp peaks, and smooth spectral behavior. It is also the most parsimonious estimator (Robinson, 1982), describing a complex process with very few parameters calculated from a small length of data. Parametric modelling avoids many of the difficulties inherent in the traditional Fourier methods, discussions

of which can be found in many books and journals (e.g., Glaser, 1993; Johansson, 1993; Pandit, 1991). Extensions of this model, e.g., ARMAX, ARX, Box-Jenkins, allow input, system, and output noise to be expressly modelled (Ljung, 1987). In particular, the ARX model includes the effect of uncertainties and noise as a white noise term.

The ARMA model has special significance since it can be derived directly from the differential equation of motion for an *N*-degree-of-freedom (DOF) system, with the damping ratio and resonant frequency as the model parameters (e.g., Gersch and Luo, 1970). A 2*n*-2*n* ARMA model is therefore a valid model for a layered soil system, or soil-structure interaction problem. The damping ratio and resonant frequency of the *N*-degree-of-freedom oscillators are contained in the 2*n* AR parameters. Phase relations are preserved in the MA parameters. The modal frequencies ξ_j, percent of critical damping ω_j, (Ghanem et al., 1991) and power participation factor p_j (Pandit, 1991; Safak, 1988) are calculated from the system poles and residues found from partial-fraction expansion of Eq. 2. The modal parameters are defined as

$$\omega_j = \frac{\sqrt{\lambda_j^2 + \delta_j^2}}{\Delta t} \tag{4}$$

$$\xi_j = \frac{\delta_j}{\sqrt{\lambda_j^2 + \delta_j^2}} \tag{5}$$

$$p_j = -r_j \text{conj}(z_j) - z_j \text{conj}(r_j) \tag{6}$$

where $\lambda = \text{Arg}(z_j)$, $d_j = -(0.5)\ln|z_j|^2$, z_j is the pole for mode *j*, r_j is the residue for mode *j*, and Δt is the digitization rate.

3.2.2 Adaptive (recursive) model estimation

Traditional methods of system estimation, both parametric and non-parametric, are strictly valid only for stationary data. A stationary signal is one whose statistics do not change with time. The commonly invoked, loose definition of stationarity requires that the variance of the signal be constant over any and all time windows. Inherent in the Fourier transformation of a time series to

the frequency domain is the averaging of the signal components over the sampling period **T**. A piece of time is frozen over this period and the assumption made that all time before and after is the same, i.e. repeated forever. The energies present at each component frequency are integrated over the entire time period **T**.

The difficulty with non-stationary signals is that these energies are changing during this period. If the frequencies present are changing over this time window, the resulting estimation, regardless of method used, will be a smeared average as if all the frequencies with a given energy were active throughout the entire period. For weakly non-stationary processes, the effect over a small time period is unimportant. If needed, the signal can be cut into relatively stationary sections and spectra found using methods specially designed for short data segments, i.e. Burg's method.

The field of adaptive filtering was formed to model non-stationary processes. As the statistics of the signal change through time, the filter "adapts" to the changing variance with new parameters that reflect the structure of the system at that point. The predicted value for the next time step can be compared with the actual value, and the difference (referred to as innovations)

$$(y_t - \hat{y}_t)^2$$

where y_t is actual output at time t, and $\hat{y}_t$ is the prediction of output at time t made at time $t\text{-}1$, will give a measure of how well the filter is doing its job. The term "innovations" is used because this information is new information that can not be predicted by the model at this particular step.

Autoregressive parameters can be sequentially estimated so that the parameters are adaptive to the changing nature of the process (Marple and Lawrence, 1987). The AR parameters are updated after each data point, tracking slowly non-stationary signals. A forgetting factor, commonly a damped negative exponential, is used so that older data carries less and less weight. A frequency domain estimation can be made at any time step by evaluating the AR parameters around the unit circle, giving the spectral representation of the behavior of the process at that time.

The most popular direct adaptive filter, or process model, is the so-called Kalman filter (Kalman, 1960; Kalman and Bucy, 1961). Sorenson (1970) points out that the Kalman approach is a direct descendant of Gauss's least squares, except now neither the signal nor the noise model must be stationary — the state may change from sample point to sample point. Nau and Oliver (1979) state that the Kalman filter is based on a dynamic AR model defined by "two concurrent random equations of motion":

$$x_t = H^T_{t-1}\Phi_t + a_t \tag{7}$$

the AR(p) equations of motion, and the "motions" of the parameters,

$$\Phi_t = \Phi_{t-1} + b_t \tag{8}$$

where p = number of prior observations utilized,
H_{t-1} = vector of p prior data observations $x_{t-1}, x_{t-2}, \ldots, x_{t-p}$,
Φ_t = vector of p AR parameters,
a_t = Gaussian white noise with 0 mean and variance σ^2
b_t = Gaussian white noise with 0 mean and covariance matrix Q.

Equation 9 estimates a value of Φ_t comprised of **p** previous parameters, through a random walk equation. The estimate uses the weighted **p** previous data points, and yields a new observation $\mathbf{x_t}$ when added to a new noise value. The least squares solution solves the equations so that the innovations (Eq. 7) — new, dynamic information that cannot be predicted — are minimized in a least squares sense each time step.

The theory behind the Kalman filter can be manipulated to yield the system parameters for the case where there is no a priori information about the noise, and even when there is no information about the input signal. The so-called extended Kalman filter has been very successfully applied to non-stationary (and non-linear) estimation problems (Ljung, 1979; Astrom and Eykhoff, 1971). The manner of application is actually straight-forward. The Kalman model is constantly updating its estimation of the dynamic process by examining the innovations. The dynamics can be due to a changing input or noise process, or it can be due to the system itself changing. The effect is a

linearization between single time steps, but if the system is changing slowly compared to the time step used, the linearization is "invisible" and the non-linear behavior is well modelled.

Chapter 4 Parametric Modeling of Lotung Data

Previous work sponsored by NIST (Glaser, 1995a) demonstrated that the MATLAB software package (Mathworks, 1993) is ideally suited for manipulation, processing, and presentation of earthquake data. MATLAB is a matrix-based system which evolved from the LINPAC and EISPAC libraries commonly used for mainframe FORTRAN numerical analysis. Complex numerical problems can be speedily solved without programming in the traditional sense.

For this study, the standard routines contained in the MATLAB System Identification Toolbox (Ljung, 1993, 1987) allowed SI to be used as a tool accessible to the geotechnical engineer. Virtually every approach and algorithm encountered in the literature by the author could be duplicated rapidly and accurately. When run on an SGI Indy workstation, all aspects of the analysis were quick enough to be interactive.

Analysis begins by determining if the event can be modelled as stationary segments. A recursive segmentation scheme, which attempted to break the data into segments with a chosen maximum variance (Ljung, 1987), is used. However, it is not possible to determine the "correct" variance a priori. In these cases a more direct method is used — the output simulated by the calculated system has to accurately model the actual measured output.

When possible the input-output data record is broken into segments based on a mechanistic understanding of the seismic event and soil behavior gained from study of the pore pressure behavior. Initially it is assumed that the various segments are basically stationary. If the stationary model can not accurately and parsimoniously simulate the segment output, a non-stationary recursive model is used. In addition, the appropriateness of the model is checked by insuring 99 percent confidence in both the whiteness of the residual autocorrelation function and the cross-correlation function between the input and output residuals (Bohlin, 1987).

The stationary SI algorithm uses a least squares estimation for the ARX model. It is necessary to estimate the number of parameters to be calculated, which is essentially estimating the degree of freedom of the soil system. There is no obvious answer to the degrees of freedom of the system,

so several verification techniques are employed to insure that a proper model order is estimated. Model order is increased in $2n$-$2n$ steps corresponding to an additional degree of freedom each. The simulated output of the model is then compared with the actual output for congruence, and the fewest parameters needed to accurately characterize the system was chosen as the system model order. Examination of the pole and zero plot insures that excessive, overlapping parameters are not included (Ljung, 1987). If the segments proved non-stationary, they are analysed using a recursive Kalman filter technique that expressly accounts for non-stationarity (Ljung, 1987).

A brief example is proved here to illustrate the ability of the SI method to correctly model a complex, time variant system. The soil system being modeled is between 47 and 17 meters deep beneath the A array. The input signal is vdha47_16e, and the actual output is vdha17_16e. The system is being modeled as a 3-DOF system

The first model used was a [6 6 1] ARX model. In this case we are making the assumption that the signals are stationary and a time-constant model can capture the mechanical behavior or the system being excited by event 16. Figure 4.1 shows the comparison between the actual output from the 30 meters of soil compared to the simulated output. It is seen that the model does very well (RMR error = 1.11) for most of the duration of strong shaking, leading to the conclusion that we have captured the soil behavior with the stationary model. However, the model has trouble matching system behavior for the first 5 seconds of strong shaking.

As discussed in Chapter 3, the natural frequency, damping factor (% of critical) and participation factor can be calculated from the ARMA system identification. The respective values for these mechanical properties based on the stationary ARX estimation is given on Table 4.1.

Table 4.1 System properties based on ARX identification.

Mode	Natural Frequency (Hz)	Damping (% of critical)	Participation Factor
1	0.82	0.18	0.10
2	3.37	0.36	-0.32
3	7.82	0.20	0.26

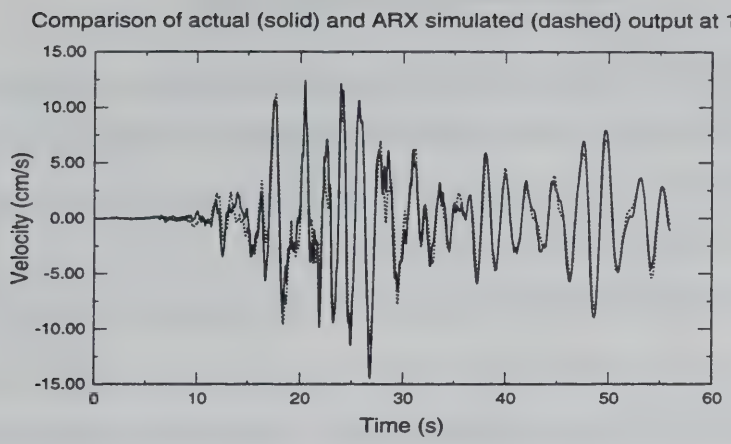

Fig. 4.1 Comparison of output simulated by stationary algorithm to actual system output.

The same soil system was then modeled using a recursive Kalman filter algorithm to see if the time-variable nature of the soil system could be captured. The results of the RARX simulation is given in Fig. 4.2. It is seen that the recursive simulation captured all aspects of the time history of the system very well (RMS error = 0.58). The amazing congruity of the simulated and actual system output attests to the fact that we can capture the mechanical behavior of the system with a few (6) simple parameters.

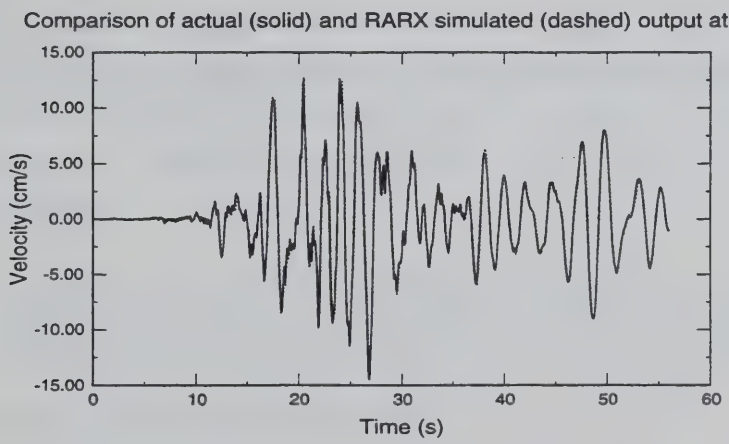

Fig. 4.2 Comparison of output simulated by recursive (nonstationary) algorithm to actual system output.

CHAPTER 5 - CONCLUSIONS

For the initial interpretation work it was decided to concentrate on the events for which accurate pore pressure records exist and show some increase in pore pressure during strong shaking. Events 12, 16, and 17 meet this criteria. A summary of the properties of these three temblors is given in Table 2. Events 12 (30 July, 1986) and 16 (14 Nov., 1986) were major events and have been discussed in detail (e.g. EPRI, 1989; Chang et al., 1991; Anderson, 1993). Event 17 is an aftershock of event 16 which generated enough pore pressure to register on the recording equipment. The time histories for acceleration, velocity, and displacement are shown in Fig. 3. The corresponding traces for the largest acceleration components for events 16 and 17 are shown in Fig. 4 and 5.

Event 7 is considered to be similar to event 12 (Elgamal, 1994), however the pore pressure transducers were not installed at this time. Event 7 is also important since it was analysed by previous researchers (Chang et al., 1989, 1990, 1991), so further analysis will build on this base of work. We will make use of this fine work by evaluating the statistical similarity of events 7 and 12. If there is stochastic congruency between the two, the evaluation of event 12 pore pressure data will further our understanding of the site response to strong motion shaking.

We are now ready to continue the application of SI to the Lotung data. If previous results are any indication, a great deal about the nonlinear behavior of earthquake excited soils will be learned (Glaser, 1995a).

CHAPTER 6 BIBLIOGRAPHY

Anderson, D.G. (1993). Geotechnical synthesis for the Lotung Large-Scale Seismic Experiment, *Report TR-102362*, Palo Alto: Electric Power Research Institute.

Bracewell, R. N. (1978). *The fourier transform and its applications*. New York: McGraw-Hill.

Bohlin, T. (1987). Model validation. *Encyclopedia of systems and control* (ed. Singh, M.) Oxford: Pergamon Press.

Chang, C.-Y., Mok, C. M., Power, M. S. (1991) Analysis of ground response data at Lotung large-scale soil-structure interaction experiment site, *Report NP-7306-M*, Palo Alto: EPRI.

Chang, C.-Y., Mok, C. M., Power, M. S., Tang, Y. K., Tang, H. T., & Stepp, J. C. (1991). Development of shear modulus reduction curves based on Lotung down-hole ground motion data. S. Prakash, ed., *Second international conference on recent advances in geotechnical earthquake engineering and soil dynamics. Vol. I*, St. Louis, MO. pp. 111-118. Rolla, MO: University of Missouri-Rolla.

Chang, C.-Y., Mok, C. M., Power, M. S., Tang, Y. K., Tang, H. T., & Stepp, J. C. (1990). Equivalent linear versus nonlinear ground response analyses at Lotung seismic experiment site. *Proc. fourth U.S. national conference on earthquake engineering. V.3* pp. 327-336. Oakland, CA: EERI.

Chang, C.-Y., Power, M. S., Tang, Y. K., & Mok, C. M. (1989). Evidence of nonlinear soil response during a moderate earthquake. *Proceedings of the twelfth international conference on soil mechanics and foundation engineering. Vol. 3,* Rio De Janeiro. pp. 1927-1930. Rotterdam: Balkema.

Converse, A.M. and Brady, A.G. (1992). BAP: basic strong-motion accelerogram processing software; version 1.0. *Open File Report 92-296A*, Denver: U.S. Geological Survey.

Elgamal, A.W., (1994). Personal communication.

EPRI (1989). Proceedings: EPRI/NRC/TPC workshop on seismic soil-structure interaction analysis techniques using data from Lotung, Taiwan, *Report NP-6154*, Palo Alto: Electric Power Research Institute.

Gersch, W., & Luo, S. (1972). Discrete time series synthesis of randomly excited structural system response. *Journal of the acoustic society of America, 51*(1), pp. 402-408.

Ghanem, R. G., Gavin, H., & Shinozuka, M. (1991). *Experimental Verification of a number of structural system identification algorithms*. p. 302. Technical Report NCEER-91-0024.

Glaser, S. (1993). *Estimating soil parameters important for lifeline siting using system identification techniques*. NISTIR 5145. p. 91. Gaithersburg, MD:NIST.

Glaser, S.D. (1995a). Insight Into Liquefaction by System Identification. *Géotechnique*. Accepted for publication.

Glaser, S.D. (1995b). System identification and its application to estimating soil properties. *ASCE Journal of Geotechnical Engineering*. July.

Johansson, R. (1993). *System identification and modeling*. Englewood Cliffs, NJ: Prentice-Hall.

Jong Shing Boring Services Company (1984). Geological Exploration and Soil Testing for EPRI/ TPC Large-Scale Seismic Testing Program. *Submitted to EPRI/TPC*.

Kalman, R. E. (1960). A new approach to linear filtering and prediction problems. *Transactions of the ASME, journal of basic engineering*, (3), pp. 35-45.

Krauss, T.P., Shure, L., & Little, J.N. (1994). *Signal processing toolbox*. Natick, MA:MathWorks.

Liu, C.C. and Yeh, Y.T. (1985). Final instrument installation report for Lotung LSST program, *Report ASIES-ER8510*, Institute of Earth Sciences, Academia Sinica.

Ljung, L. (1987). System identification: theory for the user. Englewood Cliffs, NJ: Prentice-Hall.

Ljung, L. (1979). Asymptotic behavior of the extended Kalman filter as a parameter estimator for linear systems. *IEEE transactions on automatic control, AC-24*(1), 36-50.

Ljung, L.J., (1993). *System identification toolbox*. Natick, MA: The MathWorks.

MathWorks, (1993). *MATLAB*. Natick, MA: The MathWorks.

National Taiwan University (1989). *Final testing report of foundation soils for Phase 3 Lotung LSST, Taiwan, ROC*. Submitted to the Taiwan Power Company.

National Taiwan University (1987). *Final testing report of foundation soils for Lotung nuclear power plant model, Taiwan, ROC.* Submitted to the Taiwan Power Company.

Pandit, S. M., (1991). *Modal and spectrum analysis: data dependent systems in state space.* p. 415. New York: Wiley.

Robinson, E. A. (1982). A historical perspective of spectrum estimation. *Proceedings of the IEEE,* 70(9), pp. 885-907.

Safak, E. (1988). *Analysis of recordings in structural engineering: adaptive filtering, prediction, and control.* (Open-File Report 88-647). Menlo Park, CA: U.S. Geological Survey.

Shen, C.K., and Yang, H.W. (1991). Phase III soil laboratory testing program report. *University of California - Davis.*

Shen, C.K., Chan, C.K., Li, X.S., Yang, H.W., Ueng, T.S., Wu, W.T., and Chen, C.H. (1987). Field Pore Pressure Response Measurements During Earthquakes. *University of California and Taiwan National University, submitted to the National Science Foundation/Navel Civil Engineering Laboratory, and EPRI.*

Sorenson, H. W. (1970). Least-squares estimation: from Gauss to Kalman. *IEEE spectrum,* 7(7), 63-68.

Tang, H. T. (1987). Large-scale soil-structure interaction. *Report NP-5513-SR.* Palo Alto, CA: Electric Power Research Institute.

Tang, Y.K. and Tang, H.T. (1992). Lotung Large-Scale Seismic Test strong motion records, Vol. 1-8, Report NP-7496, Palo Alto: Electric Power Research Institute.

Tang, H.T., Tang, Y.K., Stepp, J.C., Wall, I.B., Lin, E., Cheng, S.C., Lee, S.K., and Hsiau, H.M., (1989). EPRI/TPC large-scale seismic experiment at Lotung, Taiwan, *Proceedings: EPRI/ NRC/TPC workshop on seismic soil-structure interaction analysis techniques using data from Lotung, Taiwan, Report NP-6154,* Palo Alto: Electric Power Research Institute.

Wen,. K.L. and Yeh, Y.T. (1984). Seismic Velocity Structure Beneath the SMART 1 Array. *Bulletin of the Institute of Earth Science,* Academia Sinica, Vol. 4.

APPENDIX A: COMPLETE SET OF VELOCITY TIME HISTORIES FOR EVENT 16, LOCATION A.

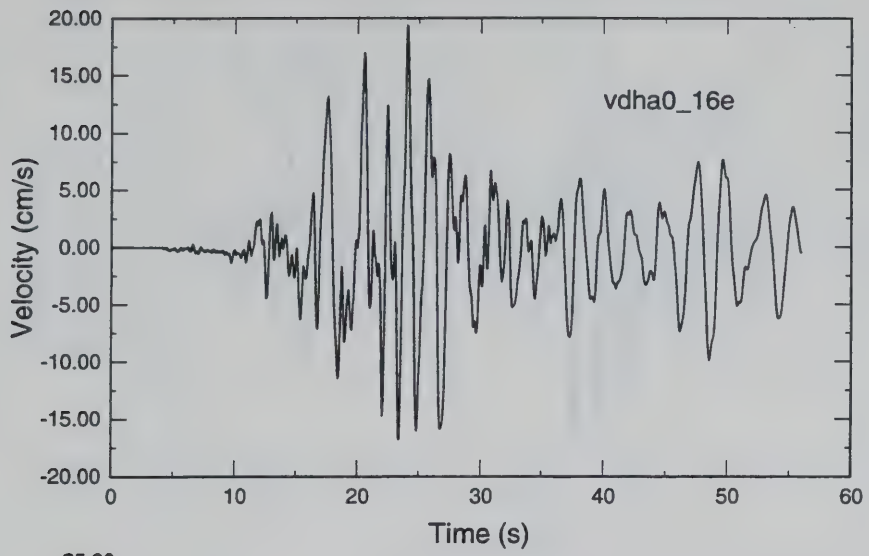
vdha0_16e
Velocity (cm/s)
Time (s)
20.00
15.00
10.00
5.00
0.00
-5.00
-10.00
-15.00
-20.00
0
10
20
30
40
50
60

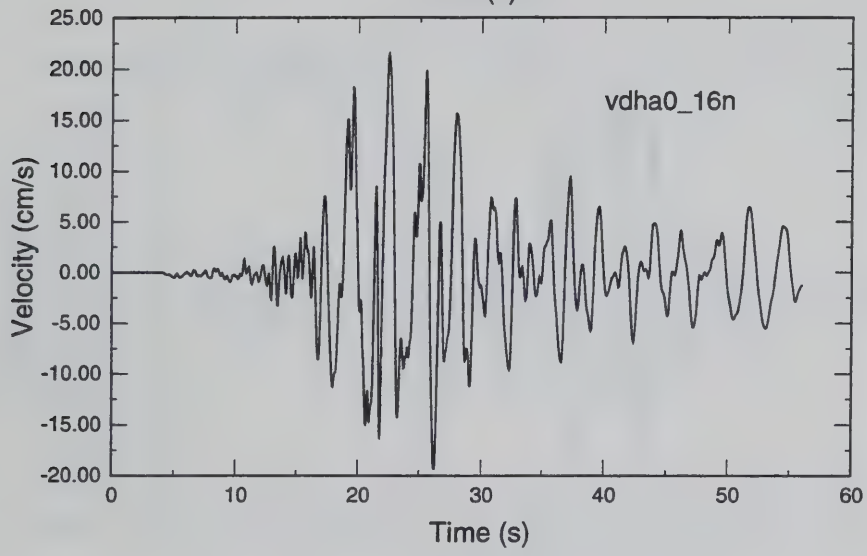
vdha0_16n
Velocity (cm/s)
Time (s)
25.00
20.00
15.00
10.00
5.00
0.00
-5.00
-10.00
-15.00
-20.00
0
10
20
30
40
50
60

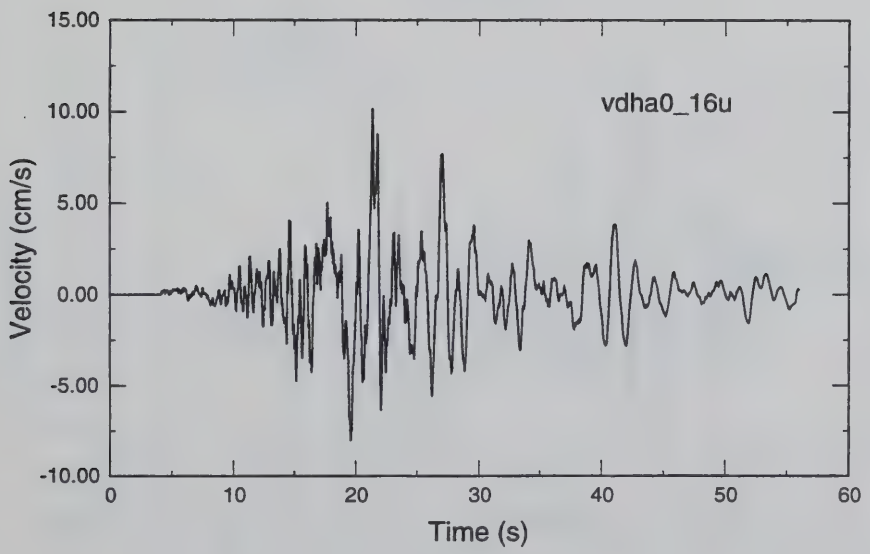
vdha0_16u
Velocity (cm/s)
Time (s)
15.00
10.00
5.00
0.00
-5.00
-10.00
0
10
20
30
40
50
60

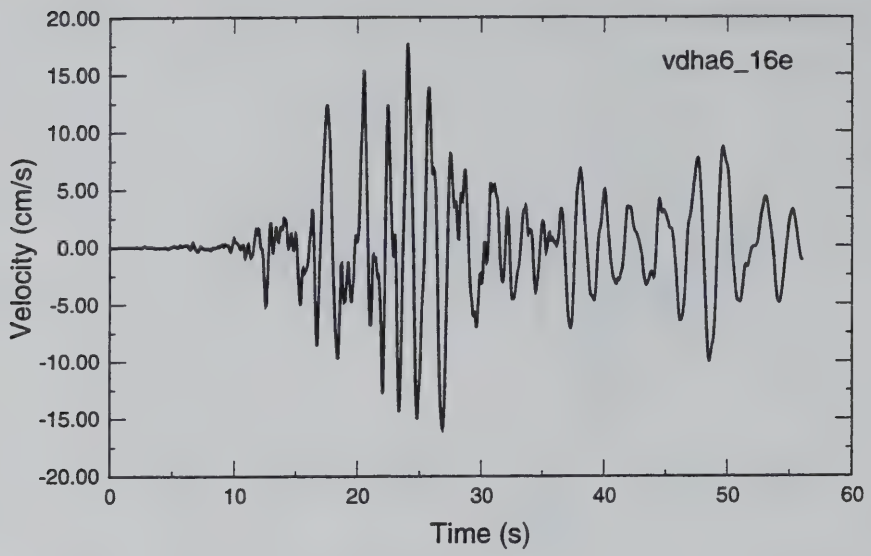
vdha6_16e
Velocity (cm/s)
Time (s)
20.00
15.00
10.00
5.00
0.00
-5.00
-10.00
-15.00
-20.00
0
10
20
30
40
50
60

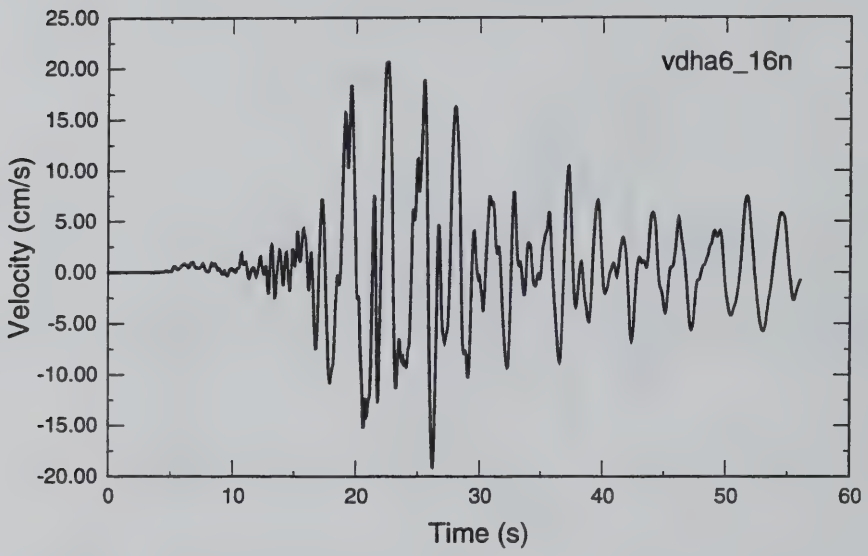
vdha6_16n
Velocity (cm/s)
Time (s)
25.00
20.00
15.00
10.00
5.00
0.00
-5.00
-10.00
-15.00
-20.00
0
10
20
30
40
50
60

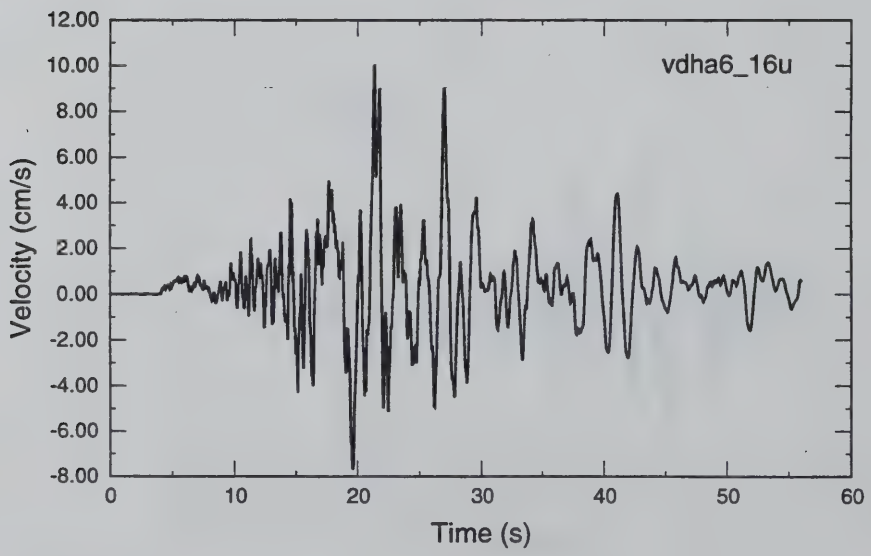
vdha6_16u
Velocity (cm/s)
Time (s)
12.00
10.00
8.00
6.00
4.00
2.00
0.00
-2.00
-4.00
-6.00
-8.00
0
10
20
30
40
50
60

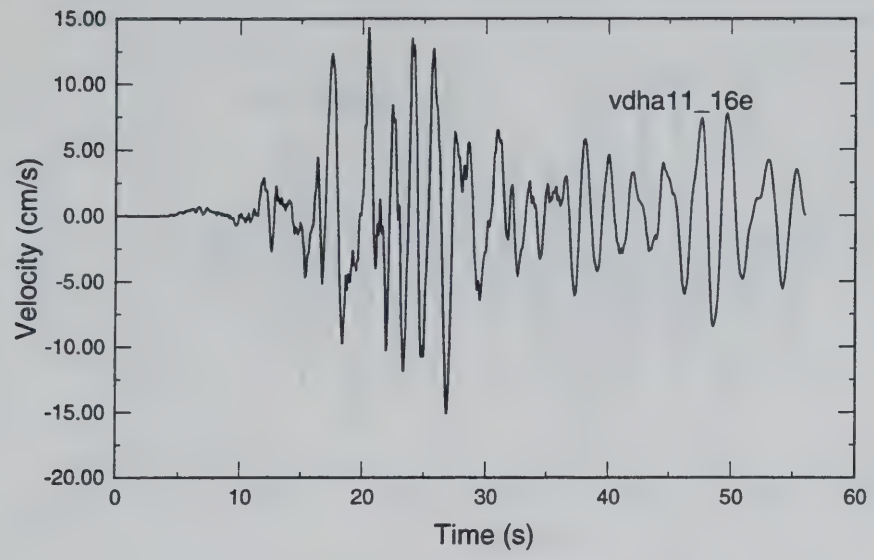
vdha11_16e
Velocity (cm/s)
Time (s)
15.00
10.00
5.00
0.00
-5.00
-10.00
-15.00
-20.00
0
10
20
30
40
50
60

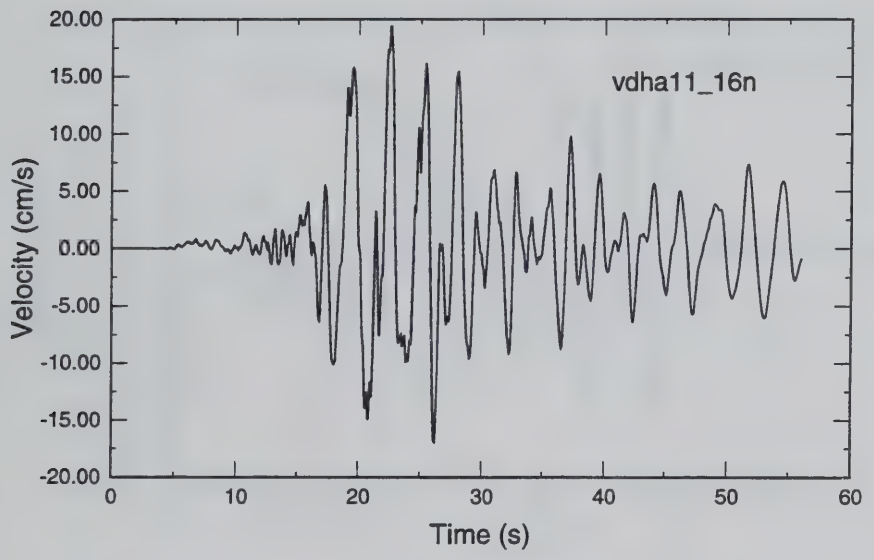
vdha11_16n
Velocity (cm/s)
Time (s)
20.00
15.00
10.00
5.00
0.00
-5.00
-10.00
-15.00
-20.00
0
10
20
30
40
50
60

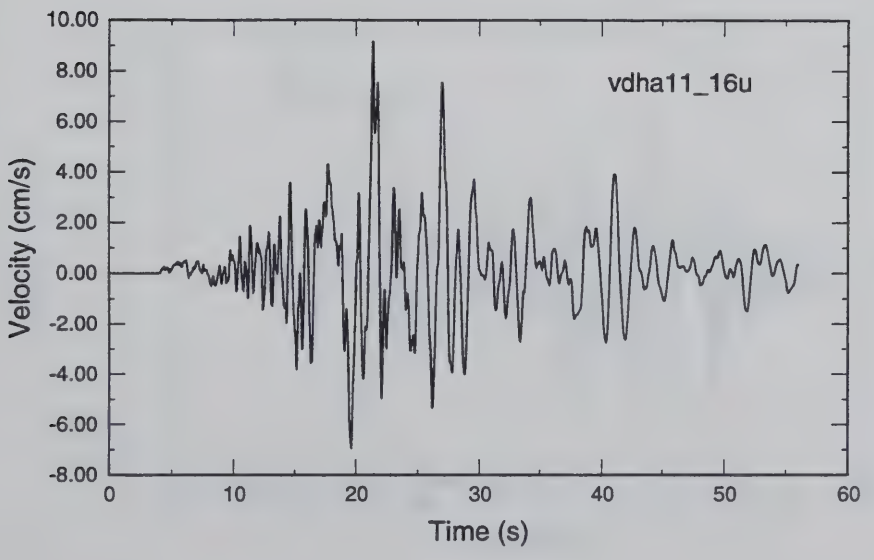
vdha11_16u
Velocity (cm/s)
Time (s)
10.00
8.00
6.00
4.00
2.00
0.00
-2.00
-4.00
-6.00
-8.00
0
10
20
30
40
50
60

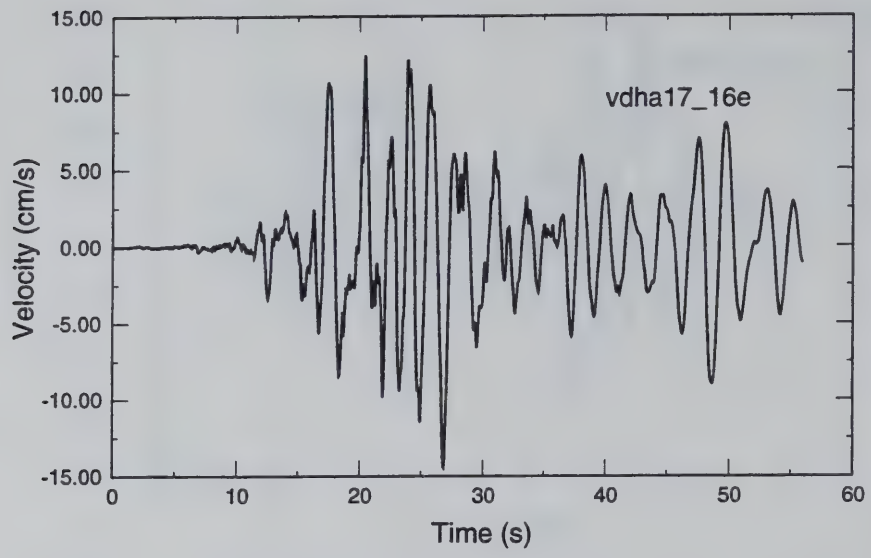
vdha17_16e
Velocity (cm/s)
Time (s)
15.00
10.00
5.00
0.00
-5.00
-10.00
-15.00
0
10
20
30
40
50
60

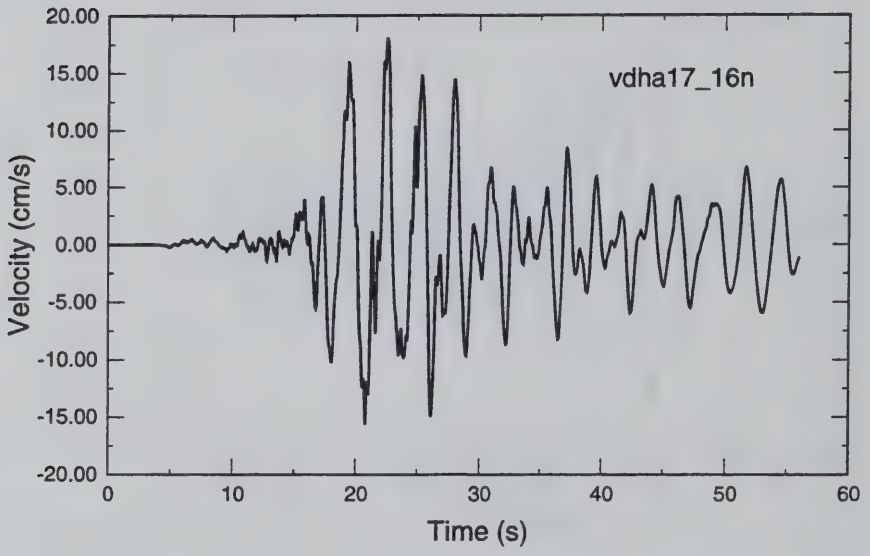
vdha17_16n
Velocity (cm/s)
Time (s)
20.00
15.00
10.00
5.00
0.00
-5.00
-10.00
-15.00
-20.00
0
10
20
30
40
50
60

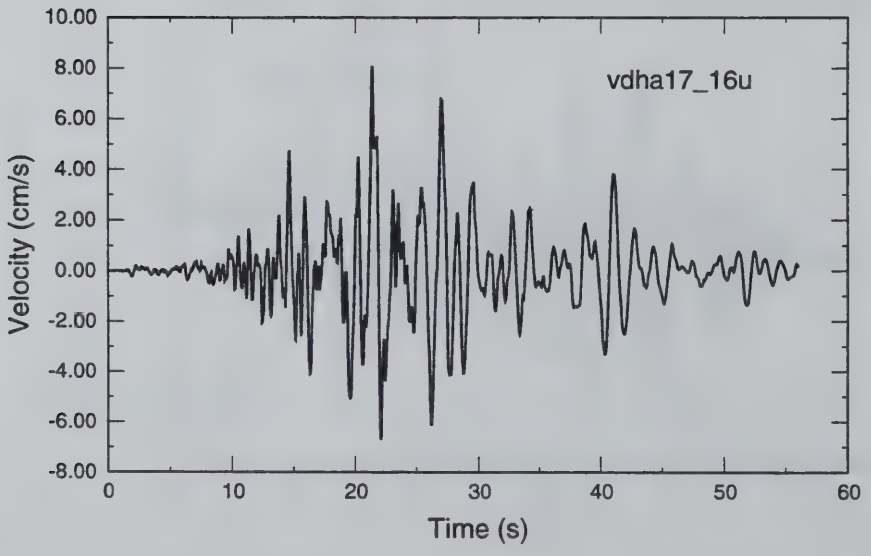
vdha17_16u
Velocity (cm/s)
Time (s)
10.00
8.00
6.00
4.00
2.00
0.00
-2.00
-4.00
-6.00
-8.00
0
10
20
30
40
50
60

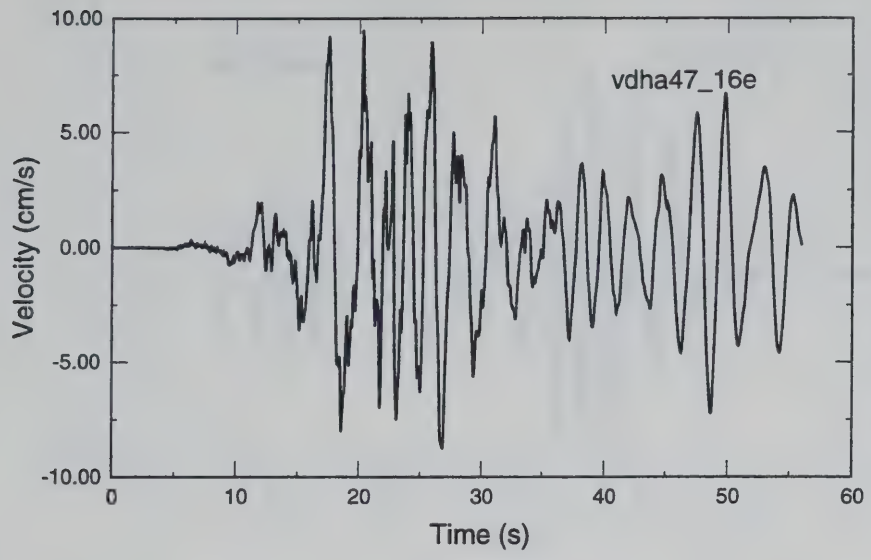
vdha47_16e
Velocity (cm/s)
Time (s)
10.00
5.00
0.00
-5.00
-10.00
0
10
20
30
40
50
60

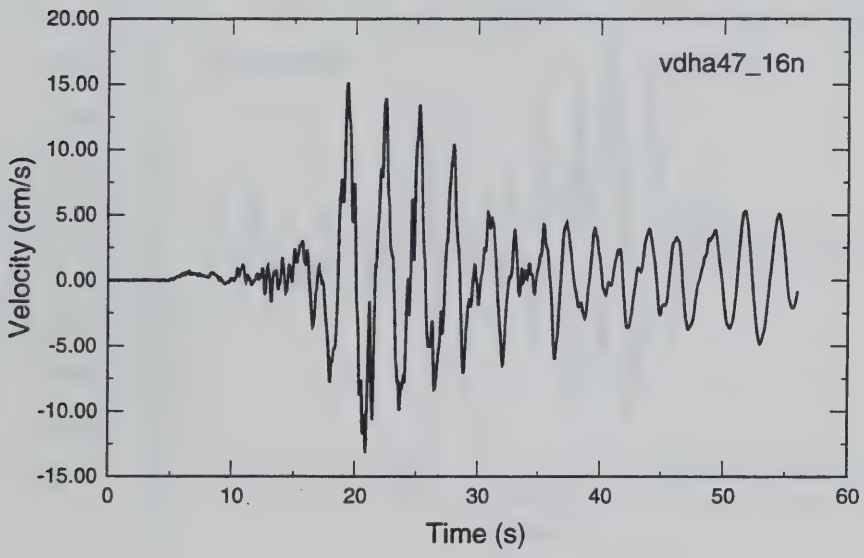
vdha47_16n
Velocity (cm/s)
Time (s)
20.00
15.00
10.00
5.00
0.00
-5.00
-10.00
-15.00
0
10
20
30
40
50
60

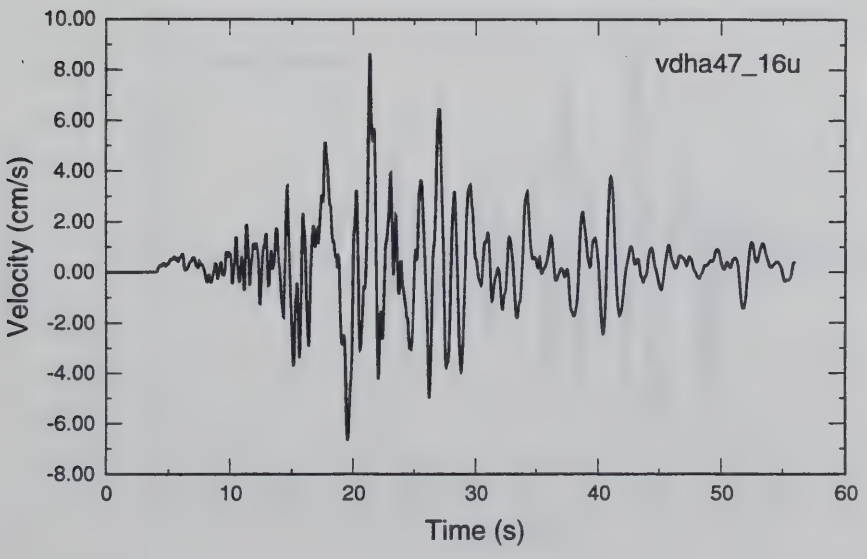
vdha47_16u
Velocity (cm/s)
Time (s)
10.00
8.00
6.00
4.00
2.00
0.00
-2.00
-4.00
-6.00
-8.00
0
10
20
30
40
50
60

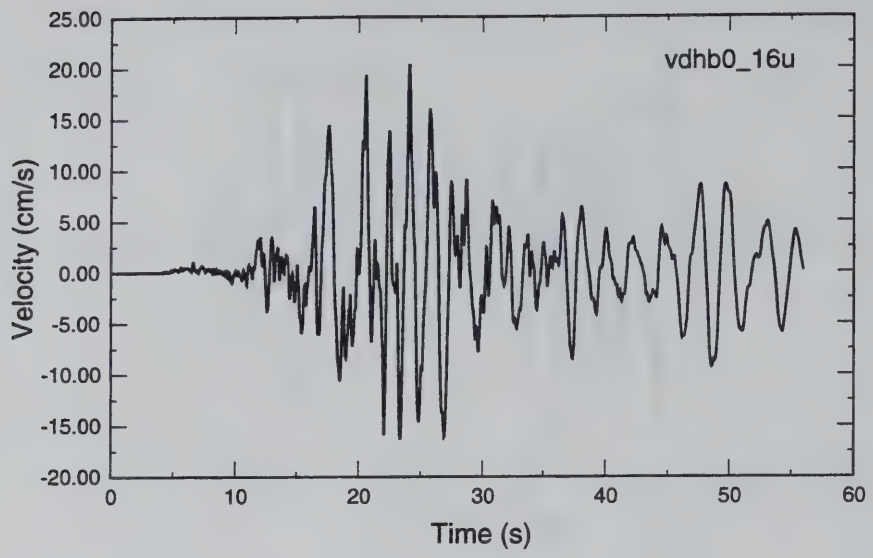
vdhb0_16u
Velocity (cm/s)
Time (s)
25.00
20.00
15.00
10.00
5.00
0.00
-5.00
-10.00
-15.00
-20.00
0
10
20
30
40
50
60

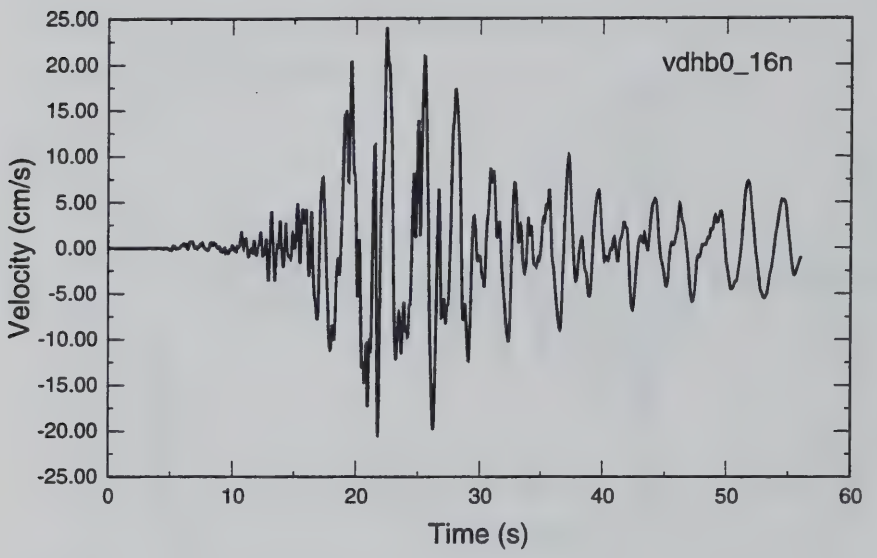
vdhb0_16n
Velocity (cm/s)
Time (s)
25.00
20.00
15.00
10.00
5.00
0.00
-5.00
-10.00
-15.00
-20.00
-25.00
0
10
20
30
40
50
60

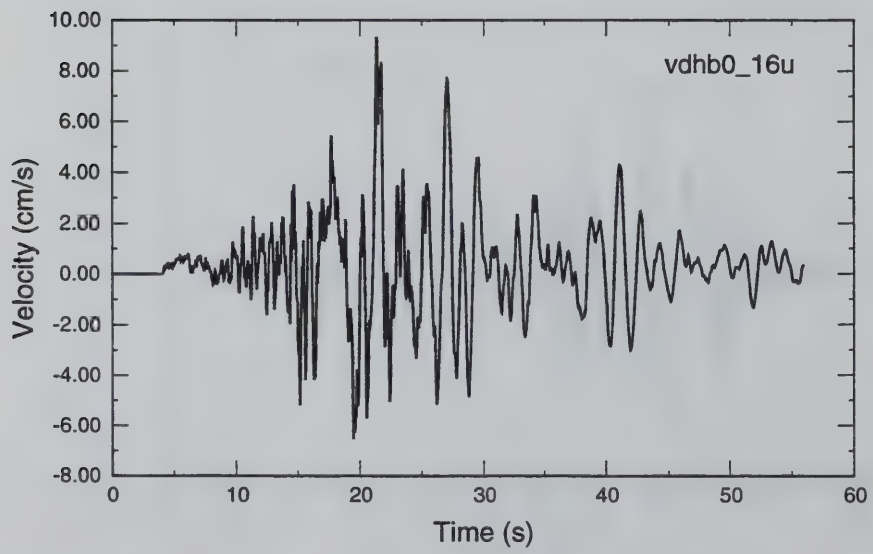
vdhb0_16u
Velocity (cm/s)
Time (s)
10.00
8.00
6.00
4.00
2.00
0.00
-2.00
-4.00
-6.00
-8.00
0
10
20
30
40
50
60

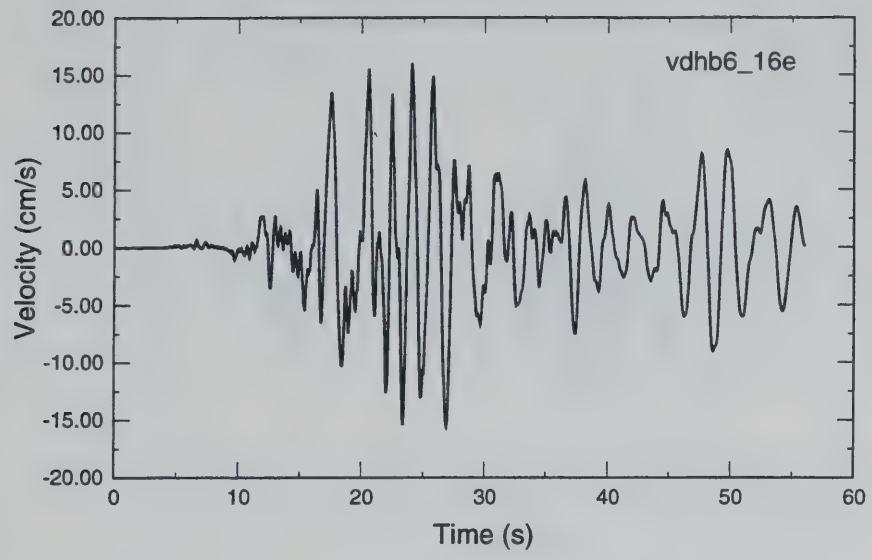
vdhb6_16e
Velocity (cm/s)
Time (s)
20.00
15.00
10.00
5.00
0.00
-5.00
-10.00
-15.00
-20.00
0
10
20
30
40
50
60

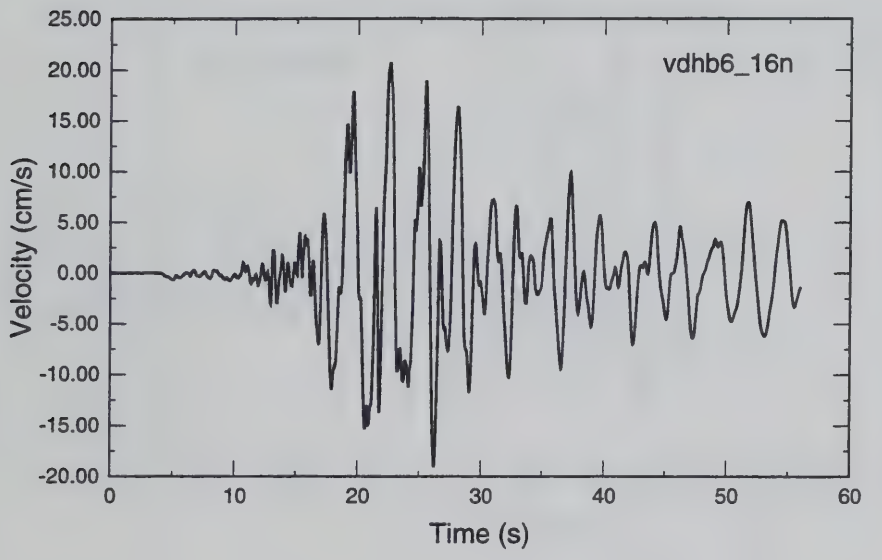
vdhb6_16n
Velocity (cm/s)
Time (s)
25.00
20.00
15.00
10.00
5.00
0.00
-5.00
-10.00
-15.00
-20.00
0
10
20
30
40
50
60

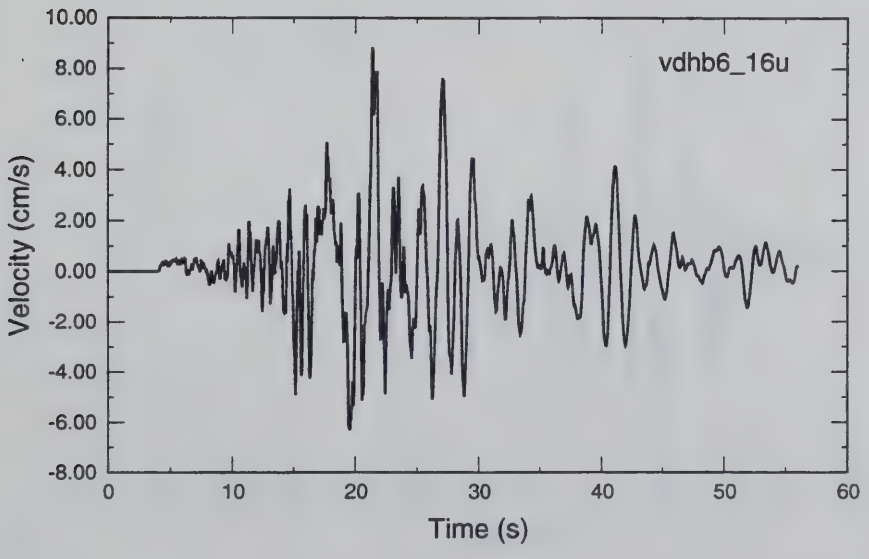
vdhb6_16u
Velocity (cm/s)
Time (s)
10.00
8.00
6.00
4.00
2.00
0.00
-2.00
-4.00
-6.00
-8.00
0
10
20
30
40
50
60

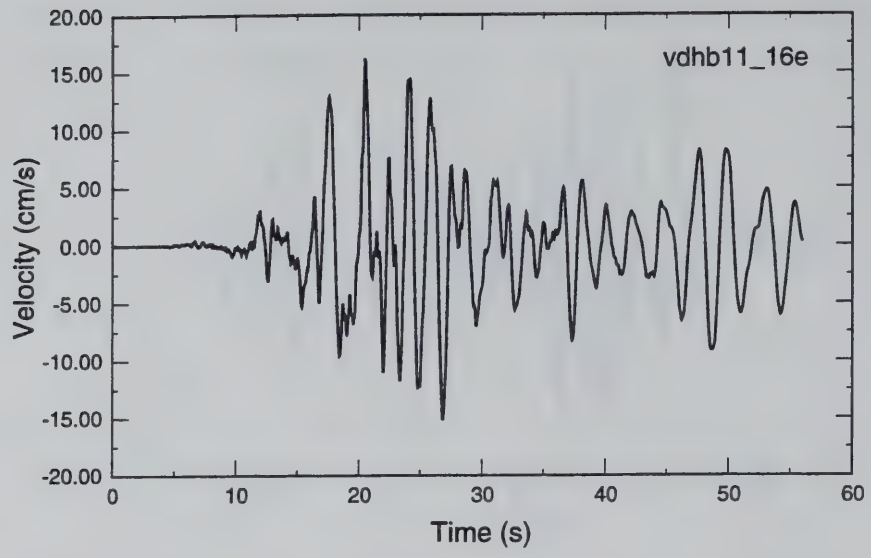
vdhb11_16e
Velocity (cm/s)
Time (s)
20.00
15.00
10.00
5.00
0.00
-5.00
-10.00
-15.00
-20.00
0
10
20
30
40
50
60

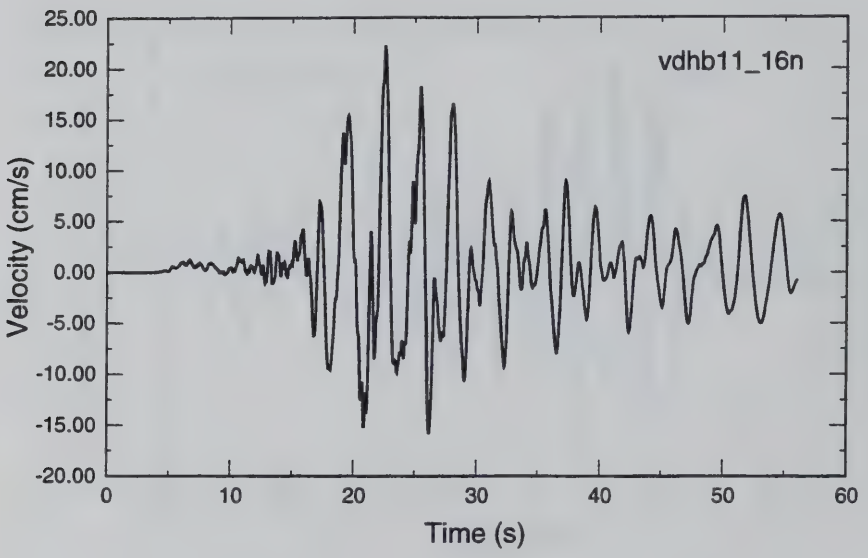
vdhb11_16n
Velocity (cm/s)
Time (s)
25.00
20.00
15.00
10.00
5.00
0.00
-5.00
-10.00
-15.00
-20.00
0
10
20
30
40
50
60

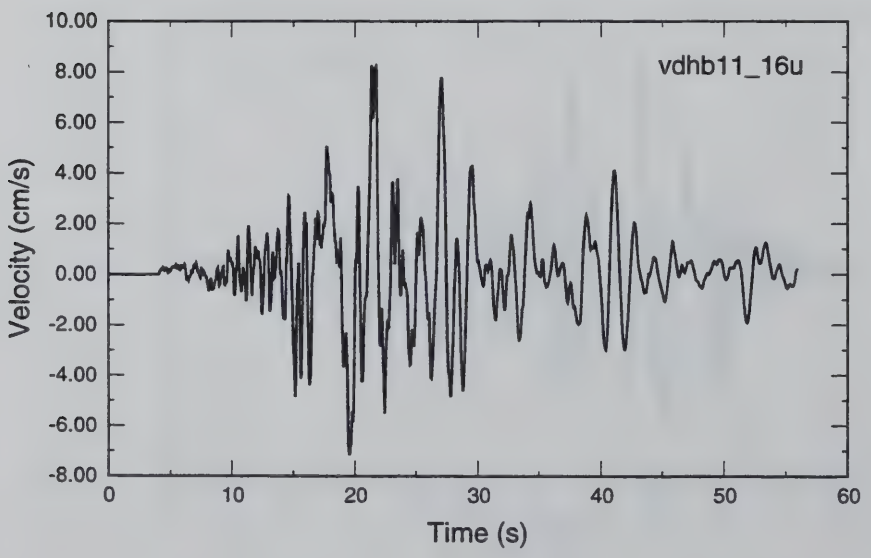
vdhb11_16u
Velocity (cm/s)
Time (s)
10.00
8.00
6.00
4.00
2.00
0.00
-2.00
-4.00
-6.00
-8.00
0
10
20
30
40
50
60

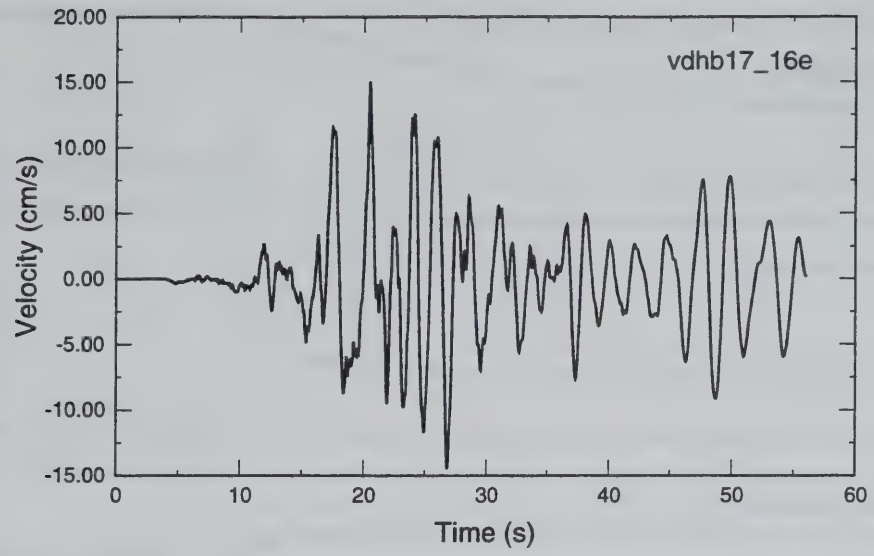
vdhb17_16e
Velocity (cm/s)
Time (s)
20.00
15.00
10.00
5.00
0.00
-5.00
-10.00
-15.00
0
10
20
30
40
50
60

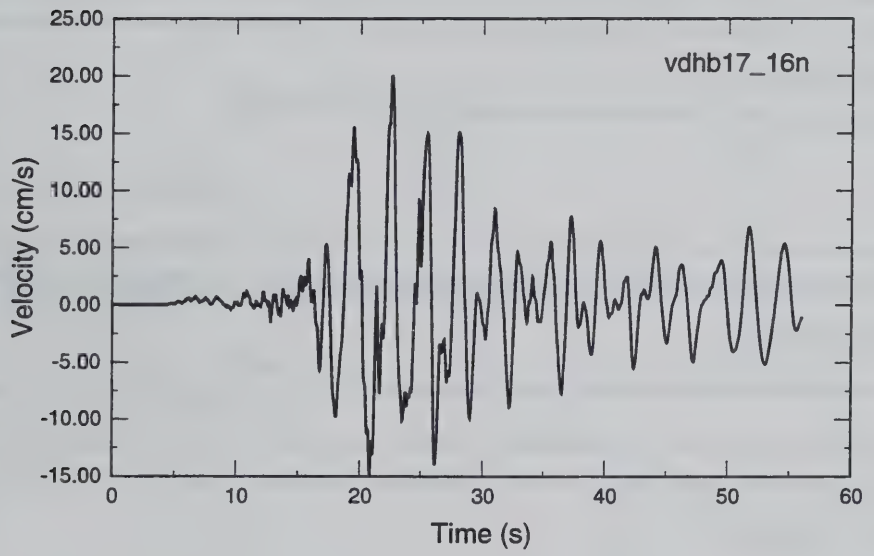
vdhb17_16n
Velocity (cm/s)
Time (s)
25.00
20.00
15.00
10.00
5.00
0.00
-5.00
-10.00
-15.00
0
10
20
30
40
50
60

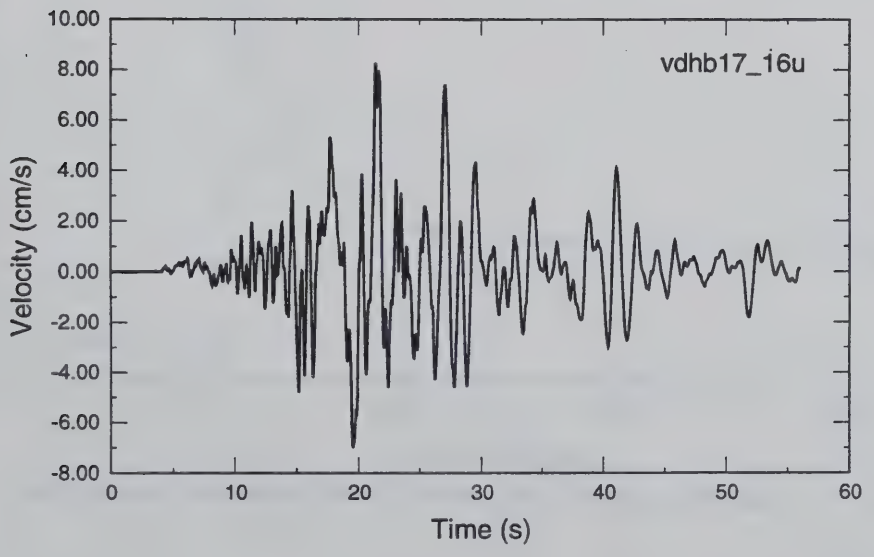
vdhb17_16u
Velocity (cm/s)
Time (s)
10.00
8.00
6.00
4.00
2.00
0.00
-2.00
-4.00
-6.00
-8.00
0
10
20
30
40
50
60

APPENDIX B: PORE WATER PRESURE TIME HISTORIES FOR EVENTS 12, 16, 17.

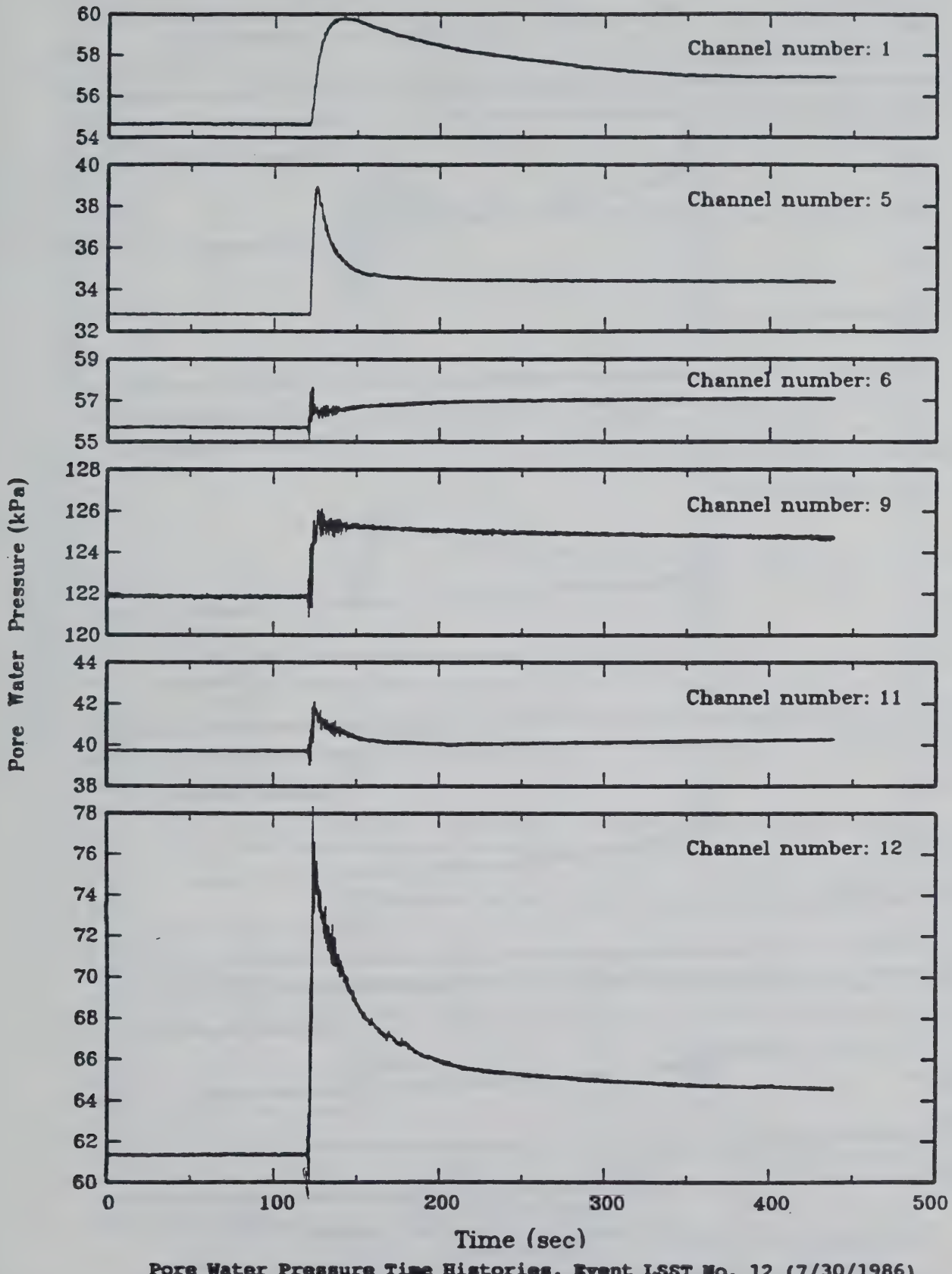

Pore Water Pressure Time Histories, Event LSST No. 12 (7/30/1986)

Tang, et al (1992)

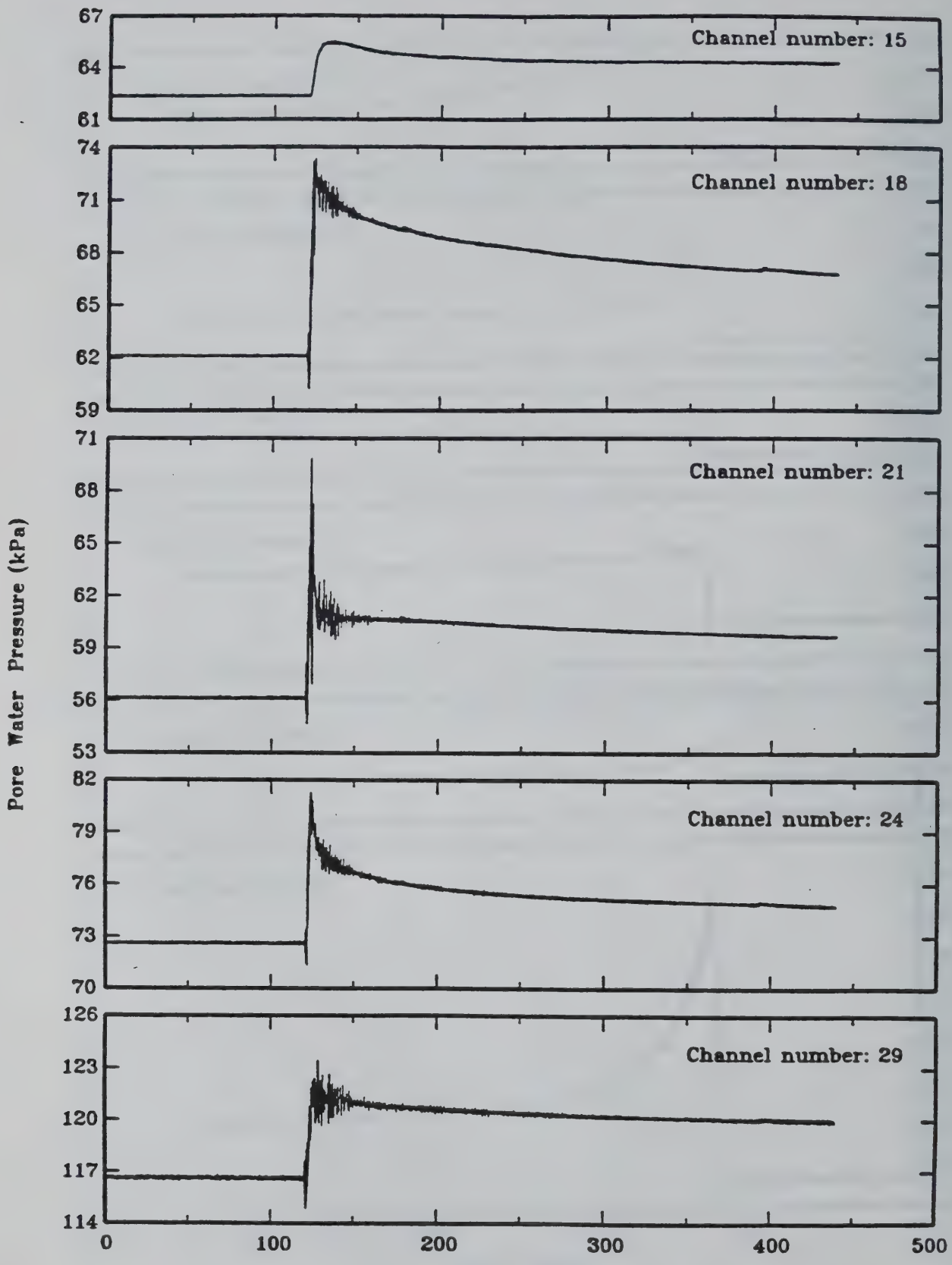

Pore Water Pressure Time Histories, Event LSST No. 12 (7/30/1986)

Tang, et al (1992)

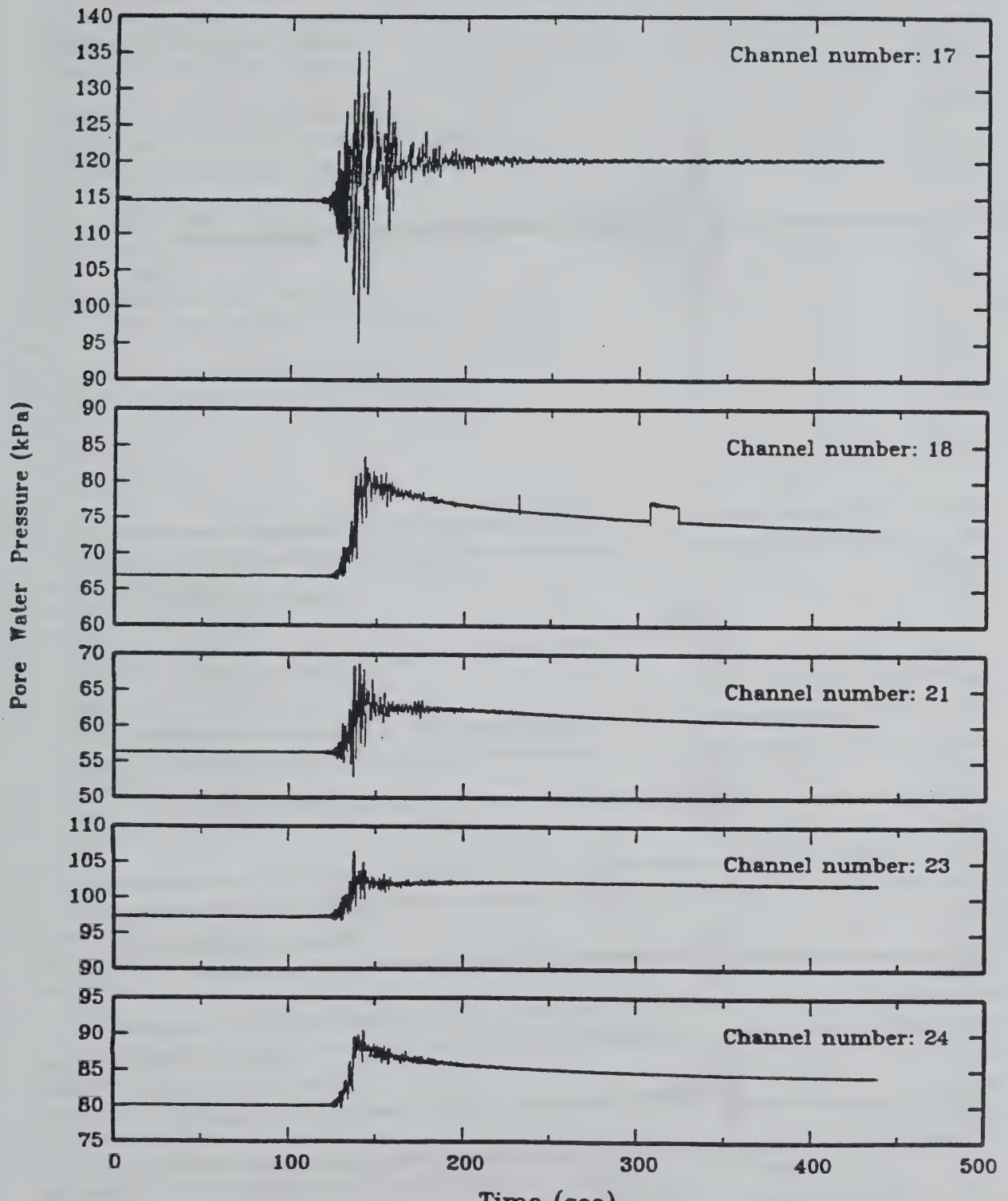

Pore Water Pressure Time Histories, Event LSST No. 16 (11/14/1986)

Tang, et al (1992)

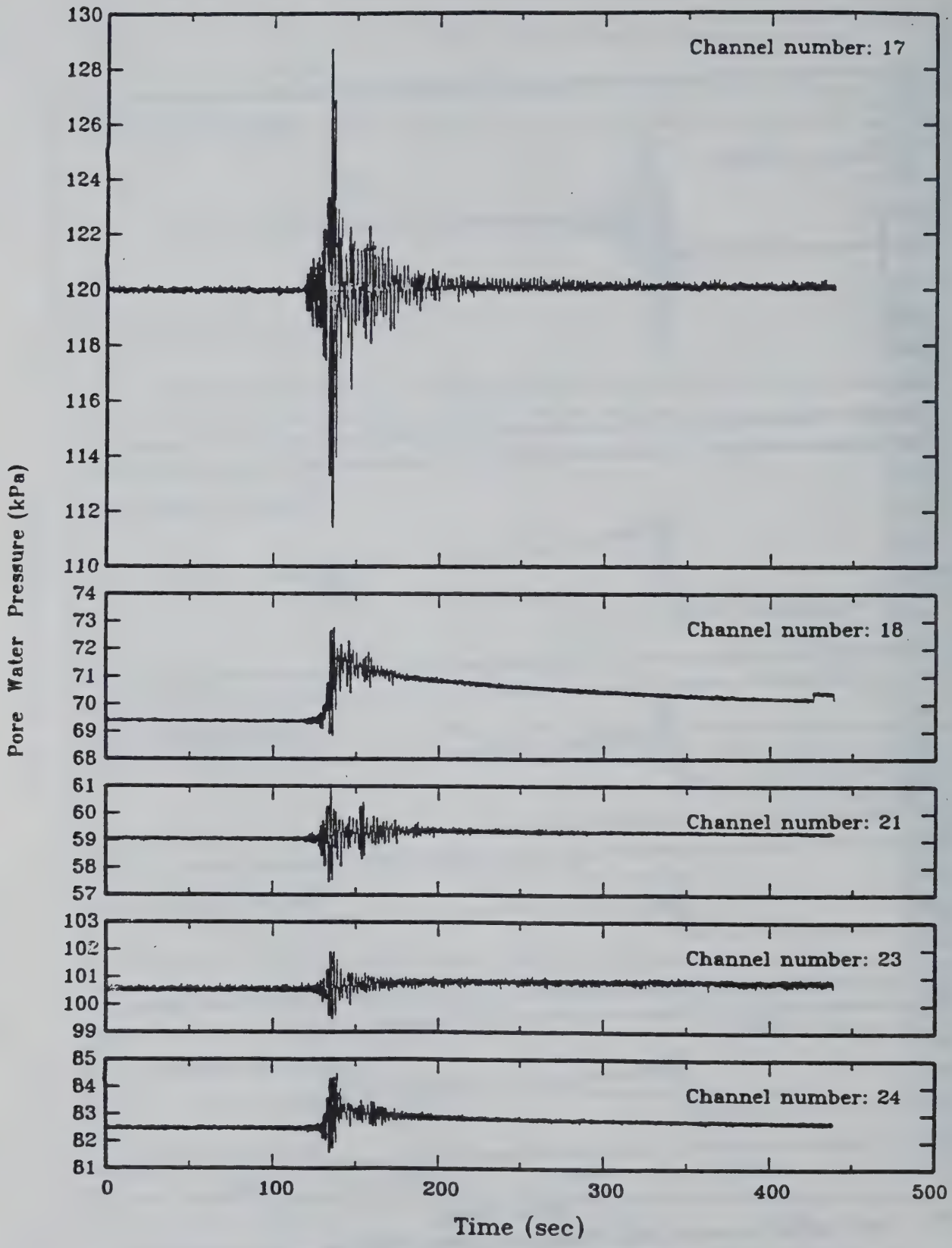

Pore Water Pressure Time Histories, Event LSST No. 17 (11/14/1986)

Tang, et al (1992)

APPENDIX C - MATLAB PROCEDURE TO INTEGRATE ACCELERATION RECORDS TO VELOCITY AND DISPLACEMENT.

```
function [a,v,d]=vd(f,Lcut,dT,n,pre,name)
% function [a,v,d]=vd(f,Lcut,dT,n,pre)
%
% detrends and filters the input acceleration,
% and integrates twice to give velocity and displacement.
% The results are plotted so they can be reviewed.
%
% f is the input acceleration vector
% Lcut is the low-end cutoff frequency in Hz.
% dT is the time step
% n is the order of the Butterworth filter;
% pre is the pre-event segment length to be zeroed.
%
% since the acceleration is filtered twice, the
% effective order of the filter is double the value of n.
%
zip=(1:pre);
zip=zeros(size(zip));
%
[b,c]=butter(n, Lcut*dT*2.0, 'high');
a=filtfilt(b,c,f);
a=dtrend(a(:,1),1,pre);
a=detrend(a);
a=a-a(pre+1);
a(1:pre)=zip;
%
v=inttrap(a,dT);
v=filtfilt(b,c,v);
v=dtrend(v(1,:)',1,pre);
v=detrend(v);
v=v-v(pre+1);
v(1:pre)=zip;
%
d=inttrap(v,dT);
[b,c]=butter(n, (Lcut*dT*2)/1.0, 'high');
d=filtfilt(b,c,d)'; d=dtrend(d(:,1),1,pre);
d=detrend(d);
d=d-d(pre+1);
d(1:pre)=zip;
%
time=(length(f)*dT)/1.0;
t=[dT: dT: time];
temp=name(1:(length(name)-6));
clf
subplot(3,1,1), plot(t,a(1:length(t))), title([temp,':  acceleration']), grid on
subplot(3,1,2), plot(t,v(1:length(t))), title([temp,':  velocity']), grid on
subplot(3,1,3), plot(t,d(1:length(t))), title([temp,':  displacement']), grid on, xlabel('Time (seconds)')
```